NAVAL SHIP RESEARCH AND DEVELOPMENT CENTER
Washington, D.C. 20007

MINIMUM ENERGY HYPERSONIC NOSE AND LEADING EDGE SHAPES

by
Roger J. Furey

AERODYNAMICS LABORATORY
RESEARCH AND DEVELOPMENT REPORT

September 1969

Report 3186

MINIMUM ENERGY HYPERSONIC NOSE AND LEADING EDGE SHAPES

The Naval Ship Research and Development Center is a U.S. Navy center for laboratory effort directed at achieving improved sea and air vehicles. It was formed in March 1967 by merging the David Taylor Model Basin at Carderock, Maryland and the Marine Engineering Laboratory at Annapolis, Maryland. The Mine Defense Laboratory, Panama City, Florida became part of the Center in November 1967.

Naval Ship Research and Development Center
Washington, D.C. 20007

NDW-NSRDC 3960/43 (10-67)

SUMMARY

A system of first-order differential equations is developed for the heat transfer (convection and shock layer radiation) and pressure drag of an axisymmetric or two-dimensional body in hypersonic flow. The Pontryagin maximum principle is applied to this system through the gradient method, and a series of optimum hypersonic nose and two-dimensional shapes of given fineness ratio is found. The optimum shapes are determined for minimum drag, minimum heat transfer (convection), minimum heat transfer (radiation), and minimum energy. The axisymmetric minimum drag shape is found similar to the 3/4 power law profile already established as the minimum drag hypersonic nose shape, and the two-dimensional result is a wedge shape. The minimum heat transfer (convection) profile, both two-dimensional and axisymmetric, is flat faced with a larger expanse of flatness in the axisymmetric case. The minimum heat transfer (radiation) is conical with a cusped tip in the axisymmetric case. Minimum energy shapes are found which minimize the sum of convection plus drag work, convection plus radiation plus drag work, and convection plus radiation. The axisymmetric results show reasonable accommodation for the various energy forms considered in each of the minimum energy nose shapes. The two-dimensional minimum energy shapes are dominated by the drag work and for all practical purposes, the results are wedge shaped.

DEPARTMENT OF THE NAVY
NAVAL SHIP RESEARCH AND DEVELOPMENT CENTER
WASHINGTON, D. C. 20007

MINIMUM ENERGY HYPERSONIC NOSE AND LEADING EDGE SHAPES

by

Roger J. Furey

September 1969 Report 3186

TABLE OF CONTENTS

LIST OF FIGURES

LIST OF TABLES

NOTATION

C_p	Specific heat at constant pressure (BTU/lb deg R) also pressure coefficient
C_v	Specific heat at constant volume (BTU/lb deg R)
D	Pressure drag (Equation [7]) (lb) also base diameter (ft) page 6
H	Hamiltonian function (Equation [54])
h	Enthalpy (BTU/lb) also coordinate parameter (Equations [13-16])
L	Characteristic length
M_∞	Mach number
N_α	Convection parameter-dimensionless (Equation [40])
N_Γ	Radiation parameter-dimensionless (Equation [41])
Pr	Prandtl number
P_i	Adjoint variables (Equation [52])
p	Pressure (lb/ft^2)
Q_c	Total convective heating rate (BTU/hr)
Q_r	Total radiative heating rate (BTU/hr)
q_c	Local convective heating rate ($BTU/hr\ ft^2$)
q_r	Local radiative heating rate ($BTU/hr\ ft^2$)
R	Radius of curvature, Figure 3, (- $1/d\theta/ds$)
R	Gas constant (BTU/lb deg R)
r	Body coordinate, Figure 2, dimensionless, $(\bar{r}/\bar{r}_b)$
$\bar{r}$	Body coordinate (ft)
$\bar{r}_b$	Base radius (ft)
S	Entropy (BTU/deg R)
s	Body coordinate (Figure 2) dimensionless $(\bar{r}/\bar{r}_b)$
$\bar{s}$	Body coordinate
T	Temperature, degree absolute (R)
$\bar{T}$	Local average temperature ratio, (Equation [39])
t	Independent variable in maximum principle formulation
U_∞	Freestream velocity (ft/sec)
u	Local velocity parallel to body surface (ft/sec)
u(t)	Control variable in maximum principle formulation
$\bar{u}$	Local average velocity ratio, (Equation [39])
v	Local velocity normal to body surface (ft/sec)

w	μ/RT
x	Axial body coordinate (Figure 2) dimensionless $(\bar{x}/\bar{r}_b)$
x_i	State variable in maximum principle formulation
$\bar{x}$	Axial body coordinate (ft)
y	Coordinate normal to body surface, Figure 2 $(y/\bar{r}_b)$
$\bar{y}$	Coordinate normal to body surface (ft)
Z	Control variable (page 5)
α	State variable representing convective heating level (dimensionless)
α_p	Planck absorption coefficient
$\bar{\alpha}$	Absorption coefficient in empirical representation of Planck coefficient (ft^2/lb deg R^5)
β	State variable representing pressure drag (dimensionless)
β_2	Velocity gradient at stagnation point $(du/ds)_{s=o}$
Γ	State variable representing radiation heating (dimensionless)
γ	Specific heat ratio
δ	Shock layer thickness
η	State variable (Equation [3])
Θ	Angle between shock slope and axis
θ	Angle between surface slope and axis (Figure 2)
κ	Curvature (1/R)
λ	State variable (Equation [38])
μ	Viscosity coefficient (lb sec/ft^2)
μ_i	Constant related to transversality condition (Equation [53])
ν	Constant related to step size in control variation (Equation [55])
ρ	Density lb./ft^3 or lb.-sec^2/ft^4
σ	Stefan-Boltzmann constant (BTU/hr ft^2 deg R^4)
τ	Optical depth
Ψ	Stream function and coordinate, (Equation [17] and Figure 3)
Ψ_i	End constraints on state variables (page 19)
$(\dot{})$	$\equiv d/ds$

Subscripts

b	Conditions at surface of body
e	Edge of boundary layer
o	Conditions at stagnation point

r	Reference conditions
s	Conditions just inside shock
t	Total conditions
1	Upstream of normal shock
2	Downstream of normal shock
∞	Freestream conditions

Superscripts

o	Initial conditions in maximum principle formulation
f	End conditions in maximum principle formulation

ABSTRACT

A system of first-order differential equations governing the heat transfer (convection and shock layer radiation) and pressure drag of an axisymmetric or two-dimensional body in hypersonic flow is developed. The Pontryagin Maximum Principle is applied to this system, through the gradient method, and a series of optimum hypersonic nose and two-dimensional shapes of given fineness ratio is found. The axisymmetric minimum drag shape is similar to the familiar 3/4 power law profile while the two-dimensional result is wedge shaped. The minimum heat transfer profiles are found to be flat faced when considering convection alone and conical, with a cusped tip, when considering radiation alone. Minimum energy shapes are found wherein the various energy terms being minimized include the sum of convection plus drag work, convection plus radiation plus drag work and convection plus radiation. The axisymmetric results show reasonable accommodation for the various energy forms considered in each of the minimum energy nose shapes. The two-dimensional minimum energy shapes are found to be dominated by the drag work with the results being, for all practical purposes, wedge shaped.

ADMINISTRATIVE INFORMATION

The work reported herein was sponsored by NAVAIR 320 under Project WR 009 0201, Task 10204.

This work was originally submitted in partial fulfillment for the degree of Doctor of Philosophy in Fluid Mechanics and Heat Transfer at the Catholic University of America, Washington, D.C. The dissertation was prepared under the direction of Dr. S.W. Chi, Assistant Professor of Fluid Mechanics and Heat Transfer and was approved by Dr. Y.C. Whang and Dr. T.W. Kao as reviewers.

INTRODUCTION

Like those of the lower speed regimes, hypersonic vehicles are designed with a particular mission in mind. The blunt shape considered optimum for reentry vehicles at near-earth orbital velocities could not be considered as optimum for a short-range hypersonic missile. The minimum drag shape that is well suited for short-range application may prove undesirable for a cruise-type vehicle which must sustain large heat loads for relatively long flight times. Under such conditions, the optimum shape would be one that accounts for both drag and heat transfer.

The use of variational methods to determine optimum aerodynamic shapes has a long and fruitful history. The minimum drag body of Newton (Figure 1) still stands as the minimum drag body of given fineness ratio at hypersonic speeds (although originally not meant specifically for this speed range). Extensive studies involving the calculus of variations have been and continue to be directed toward this problem. Minimum drag bodies of revolution with a given base diameter and internal volume, given base and surface area, and other similar geometric restrictions have been obtained through these methods.[1,2] Nose shapes that result in minimum heat transfer at supersonic and hypersonic speeds have likewise received due consideration. Much of the effort in this area has been by other than strictly variational methods,[3,4] but several studies using these methods have been undertaken[5,6] and have shown that the flat-faced body is the optimum shape for keeping convective heat transfer to a minimum.

The minimum drag and minimum heat transfer shapes of Figures 1 and 2 may be best suited for specific missions in the hypersonic speed range, but it is apparent that the cruise-type hypersonic vehicle, wherein both minimum drag and minimum heat transfer are desired, requires a compromise between the blunt heat transfer shape and the slender minimum drag profile. Such considerations lead to the concept of a minimum energy nose shape which minimizes the sum of the heat added to a given body and the work being done on that body by drag forces. Like minimum drag and minimum heat transfer, the minimum energy nose shape is also well suited to variational methods. Some effort has been expended on this particular problem; in a previous paper,[5] the author used numerical optimization methods to determine the minimum energy shape for a hypersonic body with a given base diameter and meridian arc length.

The present study will attempt to determine the minimum energy nose and leading edge shapes that have the more practical geometric restriction of a given fineness ratio and, additionally, that include in the analysis the effects of radiative heating from the shock layer to the body. Since

---

[1]References are listed on page 40.

the maximum Mach number for a hypersonic cruise vehicle would be on the order of 20 to 25, radiation heating would be a small part of the overall heating to the cruise vehicle; however inclusion of its effect in an optimization scheme may well contribute to a less blunt minimum energy shape and thereby provide an additional bonus in performance.

Minimum energy nose shapes might also be considered for superorbital reentry vehicles wherein the velocity is such that radiation heating is comparable to and eventually exceeds that of convection. Since the conical shape has been suggested as desirable to keep radiation at a minimum (by avoiding the high shock layer temperatures associated with the blunt body), a compromise is again required between the blunt shape for convection and the slender shape for radiation.

It is seen, then, that a variety of optimum shapes may exist for the hypersonic vehicle. The particular mission is the governing factor as to whether a minimum drag, a minimum heat transfer, or a minimum energy shape is most desirable. The present study is an attempt to determine such minimum energy shapes.

The problem is approached by setting up a system of first-order ordinary differential equations governing the variables of interest in the form of a Mayer problem in the calculus of variations. The formulation so established will be found rather complex for straightforward application of the calculus of variations. A numerical application of the Pontryagin maximum principle is employed and the optimum shapes determined. A geometrical restriction of a given fineness ratio is imposed on the nose and leading edge shapes. The optimum shapes include minimum drag (pressure drag), minimum heat transfer (convection), minimum heat transfer (radiation), minimum energy (convection + drag), minimum energy (convection + radiation + drag), and minimum energy (convection + radiation), all under steady-state conditions.

The flow-field analysis is made under the assumptions of an optically thin gas and a physically thin shock layer. The modified Newtonian theory provides surface pressure distribution, and centrifugal effects account for pressure variation through the shock layer. A first approximation of the flow field is obtained on the basis of an isoenergetic condition in the shock layer. The effect of radiation cooling on the temperature distribution

is calculated and radiative heating to the body determined. Convective heating is obtained with the condition that the wall temperature is much less than that at the edge of the boundary layer, thus allowing a similarity solution to the boundary layer equations. The low wall temperature is consistent with a black body assumption concerning the radiative heating.

FORMULATION OF PROBLEM

The model used employs the assumption of an inviscid shock layer. The Reynolds number is then sufficiently high so that the interaction parameter is much less than unity (i.e., $M_\infty^2/\sqrt{Re} \ll 1$). The basic hypersonic condition $M_\infty \gg 1$ is employed to justify the assumption that the shock layer is physically thin with the shock wave closely conforming to the body contour. The system of first-order differential equations governing the variables of interest is obtained as indicated below.

1. Aerodynamic Heating. The coordinate system is shown in Figure 2 with s, the distance measured along the body surface from the stagnation point, as the independent variable. The local laminar convective heat transfer rate is given[7] by:

$$q_c = 0.5\ (Pr)^{-\frac{2}{3}} \left[(\rho_e \mu_e)_o\right]^{1/2} U_\infty^{1/2}\ h_t\ \bar{r}_b^{-\frac{1}{2}}\ F(s)$$

where

$$F(s) = \frac{\left(1/2\right)^{1/2} \left(p/p_o\right)\left(u/U_\infty\right)\left(w_e/w_{e_o}\right) r^j}{\left[\int_o^s \left(p/p_o\right)\left(u/U_\infty\right)\left(w_e/w_{e_o}\right) r^{2j}\ ds\right]^{1/2}} \qquad [1]$$

The coordinates are considered as dimensionless through division by the base radius, and j = 1, 0 refers to the axisymmetric or two-dimensional case, respectively.

The total heat transferred to a given body is determined by:

$$Q_c = (2\pi)^j \bar{r}_b \bar{r}_b^{\,j} \int_o^s r^j q_c \, ds$$

Assuming $w_e \simeq w_{e_o}$, we then have:

$$\dot{\alpha} \equiv \frac{d}{ds}\left[\frac{Q_c}{\frac{Pr^{-\frac{2}{3}}}{\sqrt{2}} (2\pi)^j (\rho_e \mu_e)_o^{1/2} U_\infty^{1/2} h_t \bar{r}_b^{\,j+1/2}}\right] = \frac{\left(p/p_o\right)\left(u/U_\infty\right) r^{2j}}{\eta^{1/2}} \qquad [2]$$

where

$$\eta = \int_o^s \left(p/p_o\right)\left(u/U_\infty\right) r^{2j} \, ds \qquad [3]$$

The body surface pressure will be determined through the modified Newtonian relation:

$$C_p = C_{p_o} \sin^2 \theta$$

or

$$(p - p_\infty) = (p_o - p_\infty) Z^2 \quad \text{where } Z \equiv \frac{dr}{ds} = \sin \theta$$

for

$$M_\infty >> 1 \qquad p_\infty/p_o << p/p_o \quad \text{and} \quad p_\infty/p_o << 1$$

Then

$$\left(p/p_o\right) \simeq Z^2 \qquad [4]$$

The convective heating equations (Equations [2] and [3]) can then be expressed as:

$$\dot{\alpha} = \left({}^{u}/_{U_\infty}\right) Z^2 \; r^{2j}/\eta^{1/2} \qquad [5]$$

$$\dot{\eta} = \left({}^{u}/_{U_\infty}\right) Z^2 \; r^{2j} \qquad [6]$$

It remains to determine the local velocity ratio in a convenient form. This will be delayed until consideration of the shock layer radiation terms.

2. Aerodynamic Drag. In the body-oriented coordinate system of Figure 2, the pressure drag of an arbitrary body can be expressed as:

$$D = (2\pi)^j \; \bar{r}_b \; \bar{r}_b{}^j \int_o^s (p - p_\infty) \; r^j \sin\theta \; ds$$

or

$$\beta = \left[\frac{D}{(2\pi)^j \; \bar{r}_b \; \bar{r}_b{}^j \; p_o}\right] = \int_o^s \left({}^{p}/_{p_o} - {}^{p_\infty}/_{p_o}\right) r^j \; Z \; ds \qquad [7]$$

On the assumption that ${}^{p_\infty}/_{p_o} \ll {}^{p}/_{p_o}$ in the nose region and substituting Equation [4], the drag relation becomes:

$$\dot{\beta} = Z^3 \; r^j \qquad [8]$$

3. Shock Layer. The radiation term in the energy equation for an optically thin gas[8] is:

$$\nabla \cdot \vec{q}_r = 4 \; \alpha_p \; \sigma \; T^4 \qquad [9]$$

Unlike the equations related to convective heating (Equations [5] and [6]) and pressure drag (Equation [8]) wherein the history of the variables is

needed on the body surface only, the temperature distribution of Equation [9] is needed throughout the shock layer. There are several numerical solutions for a blunt body shock layer flow, but they are unsatisfactory for the problem at hand either because they are indirect or inordinately time consuming. The numerical optimization procedure to be used necessitates recalculating the shock layer properties (in those problems where radiation is being considered) after each iteration, with each resultant new shape closer to the optimum. Since there are many such intermediate shapes between the initial assumed optimum and the final optimum shape, a direct and rapid calculation of the shock layer properties is a must in order to keep machine time within reason. The shock layer model to be used will be similar to that of Freeman[9] but modified to avoid the possibility of a free layer (negative pressure on the body surface) inherent in his treatment on some types of bodies.

The continuity of mass, momentum, and energy across an oblique shock provides:

$$\begin{aligned} \rho_1 U \sin\Theta &= \rho_2 v \\ p_1 + \rho_1 U^2 \sin^2\Theta &= p_2 + \rho_2 v^2 \\ h_1 + 1/2\, U^2 \sin^2\Theta &= h_2 + 1/2\, v^2 \\ U \cos\Theta &= u \end{aligned} \qquad [10]$$

For $M_\infty >> 1$, the dynamic terms on the upstream side are much larger than the static terms; thus:

$$\begin{aligned} \rho_1 U \sin\Theta &= \rho_2 v \\ \rho_1 U^2 \sin^2\Theta &= p_2 + \rho_2 v^2 \\ 1/2\, U^2 \sin^2\Theta &= h_2 + 1/2\, v^2 \\ U \cos\Theta &= u \end{aligned} \qquad [11]$$

from which it can be determined:

$$v = \frac{\gamma - 1}{\gamma + 1} U \sin \Theta + 0\left[\frac{1}{M^2}\right]$$

$$\rho_2 = \rho_1 \frac{\gamma + 1}{\gamma - 1} + 0\left[\frac{1}{M^2}\right] \qquad [12]$$

$$p_2 = \frac{2}{\gamma + 1} \rho_1 U^2 \sin^2 \Theta$$

Consider now the specific heat ratio; from the kinetic theory of gases, this can be expressed as:

$$\gamma = \frac{\xi + 2}{\xi}$$

where ξ represents the degrees of freedom within the gas. At the higher shock layer temperatures associated with hypersonic speeds, the degrees of freedom increase as the real gas effects of vibration, dissociation, etc. come into play. As $M_\infty \to \infty$, then, it follows that $\gamma \to 1$. Although the specific heat ratio does, in fact, never reach unity, the assumption of such a limit provides for considerable simplification in the shock layer equations. Then, through Equations [12], the shock relations lead to the conclusion that the normal component of velocity approaches zero while the shock layer density becomes infinite.

Freeman[13] proceeded on the assumption that the shock layer variables were everywhere of the same order of magnitude as the values just behind the shock. He developed what amounted to a series approximation for the desired variables in terms of $\varepsilon = \rho_1/\rho_2 \simeq (\gamma - 1)/(\gamma + 1)$. This leads to the Newton-Busemann pressure relation for the surface pressure distribution. For bodies of sufficient curvature, this relation results in the previously noted free layer, an unacceptable drawback when it is not known a priori (as in the present case) exactly what shape or shapes must be dealt with. The modified Newtonian pressure relation is known to correlate very well with experiment over a wide range of supersonic through hypersonic Mach numbers and body shapes and does not have the free-layer difficulty. For this reason and in order to be consistent with the development of the convective heating and drag equations, the modified Newtonian relation will be used in determining the surface pressure while the other features of the Freeman model will be maintained in developing the shock layer solution.

The treatment of the radiation terms will be similar to that of Wang[10] who used the following assumptions:

1. Gas in local thermodynamic equilibrium.
2. Optically thin gas or the grey gas approximation.
3. Transparent shock and black wall.
4. Perfect gas.

The conservation equations in boundary layer-type coordinates consistent with Figure 2 are:[11]

$$\text{mass} \quad \frac{\partial}{\partial s}(r^j \rho u) + \frac{\partial}{\partial y}(h\, r^j\, \rho\, v) = 0 \qquad [13]$$

$$\text{s-momentum} \quad \frac{u}{h}\frac{\partial u}{\partial s} + v\frac{\partial u}{\partial y} + u\, v\, \kappa = -\frac{1}{h\rho}\frac{\partial p}{\partial s} \qquad [14]$$

$$\text{y-momentum} \quad \frac{u}{h}\frac{\partial v}{\partial s} + v\frac{\partial v}{\partial y} - u^2\, \kappa = -\frac{1}{\rho}\frac{\partial p}{\partial y} \qquad [15]$$

$$\text{energy} \quad \rho\, T\left(\frac{u}{h}\frac{\partial S}{\partial s} + v\frac{\partial S}{\partial y}\right) = -\nabla \cdot \vec{q}_r \qquad [16]$$

Through the introduction of a stream function Ψ, the continuity equation is satisfied directly.

$$\frac{\partial \Psi}{\partial s} = -h\, r^j\, \rho\, v \qquad \frac{\partial \Psi}{\partial y} = r^j\, \rho\, u \qquad [17]$$

Transforming to a Von Mises coordinate system, i.e., $(s,y) \rightarrow (s,\Psi)$, (Figure 3) through

$$\frac{\partial}{\partial s} = \frac{\partial}{\partial s} - h\, r^j\, \rho\, v\frac{\partial}{\partial \Psi} \qquad [18a]$$

and

$$\frac{\partial}{\partial y} = r^j\, \rho\, u\frac{\partial}{\partial \Psi} \qquad [18b]$$

Equations [14] through [16] reduce to:

$$u\frac{\partial u}{\partial s} + v\frac{\partial u}{\partial s} = -\frac{1}{\rho}\frac{\partial p}{\partial s} \qquad [19]$$

$$r^j\frac{\partial p}{\partial \Psi} = u\, \kappa - \frac{1}{h}\frac{\partial v}{\partial s} \qquad [20]$$

$$\rho\, T\frac{u}{h}\frac{\partial S}{\partial s} = -\nabla \cdot \vec{q}_r \qquad [21]$$

where, from Equation [9], $\nabla \cdot q_r = 4\,\alpha_p\,\sigma\,T^4$ and Equation [21] becomes:

$$\frac{1}{h}\frac{\partial S}{\partial s} = -\frac{4\,\alpha_p\,\sigma\,T^4}{\rho\,u\,T} \qquad [22]$$

An estimate of the effects of radiation on the shock layer properties and structure can be obtained as follows.

By definition the optical thickness is $\tau \equiv \int \alpha\, d\,\ell \simeq \tilde{\alpha}\, L$. Near the stagnation point, where radiation will be greatest, the shock relations provide $\rho_1\, U_1 = \rho_2\, U_2$. And as $M_\infty \to \infty$, $\gamma \to 1 \Rightarrow C_p \simeq C_v$; also $h = 1 + {}^{\gamma}/_{R} \simeq 1$.

substituting into Equation [22], we obtain

$$\frac{\partial}{\partial s}\left(\frac{S}{C_v}\right) \simeq 4\left(\frac{\tau}{L}\right)\left(\frac{\sigma\,T_2^4}{\rho_\infty\,U_\infty\,C_p\,T_2}\right) \qquad [23]$$

The first expression in parentheses on the right-hand side of Equation [23] is referred to as the optical depth and the second is the inverse of the Boltzman number. For optically thin gases and moderate hypersonic Mach numbers:

$$\left(\frac{\tau}{L}\right) << 1 \quad \text{and} \quad \frac{\sigma\,T_2^4}{\rho_\infty\,U_\infty\,C_p\,T_2} << 1$$
$$\therefore \frac{\partial}{\partial s}\left(\frac{S}{C_v}\right) \simeq 0 \qquad [24]$$

or the entropy is constant along streamlines. The implication here is that the shock layer properties can be determined through the momentum Equations ([19] and [20]) and the equation of state, and, having the temperature distribution, the radiation heating can be determined without ever considering radiation in the conservation equations. The effect here would be to overestimate the radiative contribution (however slightly) by neglecting the radiative cooling within the shock layer and the resultant temperature decrease. A more reasonable approach is that of superposition, i.e., first

determining the pressure and velocity distributions and then using these values to determine temperature distributions while including radiation. The validity of such an approach is borne out by the results of Reference 10; Wang applied the thin shock layer series approximation of Freeman and showed that, to a first approximation, the velocity and pressure distribution within the shock layer are not affected by radiation. This approach is further justified on the basis of other results that concerned considerably higher radiation levels than in the present problem. It has been observed[12] that the radiation serves to lower the local temperature while increasing the density but that it has little effect on the velocity and pressure distribution.

The approach used here, then, is to deal with Equation [19] and [20] on the basis of the isoenergetic implications of Equation [24]. Once the necessary distribution of shock layer variables is determined, Equation [22] is solved to obtain the desired temperature distribution while including the effects of radiative cooling.

Proceeding on the basis of the thin shock layer approximation and the related implications of Equations [12], the flow within the shock layer is predominately parallel to the surface, or $v \ll u$. Based on this assumption, Equations [19] and [20] reduce respectively to:

$$u \frac{\partial u}{\partial s} = - \frac{1}{\rho} \frac{\partial p}{\partial s} \qquad [25]$$

$$r^j \frac{\partial p}{\partial \Psi} = u \kappa \qquad [26]$$

Through Equation [24], Equation [25] can be expressed as:

$$\left(\frac{p_2}{\rho_2{}^\gamma}\right)^{\frac{1}{\gamma}} \int_{p_2}^{p} p^{\frac{1}{\gamma}} \frac{\partial p}{\partial s} ds = - \int_{\beta_2 s}^{u} u \frac{\partial u}{\partial s} ds \qquad [27]$$

where the reference pressure and density are those values existing in the stagnation region. The integration here then is dealing with the body-wetting streamline. The lower limit of integration for the velocity term $\beta_2 s$ is based on the fact that in the stagnation region, the velocity varies

linearly with distance. The value of β_2, i.e., $\beta_2/U_\infty = (1.268\ \sqrt{\rho_1/\rho_2})/D$ (Reference 11), is found to hold for a variety of shapes from spherical to flat faced--both axisymmetric and two-dimensional. Since the pressure p_2 is pretty much constant in the stagnation region, the corresponding lower limits are not inconsistent.

Consider now the momentum relation across a normal shock at the stagnation point (Equation [11]). The dynamic pressure on the upstream side and the static pressure on the downstream side can be said to be dominant at extreme Mach numbers. Two conclusions can be drawn from this condition, i.e.,

$$p_{t_2} \simeq p_2 \quad \text{and} \quad \frac{p_2}{\rho_2 U_\infty^2} \simeq \rho_1/\rho_2$$

where

$$\rho_1/\rho_2 \simeq \frac{\gamma - 1}{\gamma + 1} \quad \text{for} \quad M_\infty >> 1$$

Utilizing these conditions and the surface pressure from Equation [4], Equation [23] can be integrated and reduced to:

$$u/U_\infty = \left[\left(\frac{\beta_2 s}{U_\infty}\right)^2 + \frac{2\gamma}{\gamma + 1}\left(1 - Z\,\frac{2(\gamma - 1)}{\gamma}\right)\right]^{1/2} \qquad [28]$$

Equation [28] provides the velocity variation along the body wetting streamline and, together with Equations [5] and [6], provides the necessary forms for dealing with the convective heating in the Mayer problem formulation. (The form of Equation [28] shows the effect of the chosen integration limits, i.e., the introduction of $\beta_2 s$ avoids the o velocity on a flat-faced body usually associated with the Newtonian pressure approximation. The independent variable s in this equation is not varied throughout its range but only for the duration of the initial curvature existing at the stagnation point).

It remains to determine the flow properties through the shock layer so as to deal with the radiative heating.

Maslen[13] used Equation [26] to determine the shock layer properties by treating the problem through the inverse method. On assuming a shock

shape, he used the shock relations to provide the variables just inside the shock wave. The pressure gradient through the shock layer (as provided by Equation [26] using values from the shock relations) is assumed constant. Integration proceeds from the shock to the body with $\Psi = 0$ determining the body shape for the assumed shock. A similar procedure will be used in the present application except that the integration will proceed from body to shock. Equations [4] and [28] provide the values of the necessary variables and boundary conditions at the body surface. As with the Maslen method, the pressure gradient will be considered constant across the shock layer.

$\therefore$ Equation [26]

$$\int_{p_b}^{p} dp = \int_{\Psi_o}^{\Psi} \frac{u}{r^j R} d\Psi = \frac{\rho_\infty U_\infty}{R} u \int_o^s Z \, ds \qquad [29]$$

where the thin shock layer conditions have been used to change the integration variable, i.e., by definition

$$\Psi = \frac{1}{1 + j} \rho_\infty U_\infty r^{1+j}$$

where

$$r = r_b + y \cos \theta \simeq r_b$$

$$\therefore d\Psi = \rho_\infty U_\infty r_b^j Z \, ds$$

Utilizing Equation [28] in the form

$$\left(u/U_\infty\right) = f(s, Z)$$

Equation [29] can be integrated to provide

$$\frac{p(s, s_s)}{\rho_\infty U_\infty^2} = Z^2 + \frac{f(s, Z)}{R} \int_o^s Z \, ds \qquad [30]$$

where the modified Newtonian relation (Equation [4]) has been used to provide the pressure on the body surface. The Ψ dependence of the pressure is

accounted for by the subscripted s_s which refers to the entry point of a particular streamline into the shock layer. The entropy level for a particular streamline can be determined from the shock relations in the form:[14]

$$\frac{\Delta S}{C_v} = \ell n\left[\frac{2\gamma M^2Z^2 - (\gamma-1)}{\gamma + 1}\right] - \gamma\, \ell n\left[\frac{(\gamma + 1)M^2Z^2}{(\gamma - 1)M^2Z^2 + 2}\right] \qquad [31]$$

Then

$$\rho = f(\Psi)\, p^{\frac{1}{\gamma}}$$

which, together with Equation [30], will provide the density distribution through the shock layer.

The velocity at the shock wave is provided by the constancy of the tangential velocity component across the shock (Equation [11]), i.e.,

$$u_s/_{U_\infty} = \cos\Theta \simeq (1 - Z^2)^{1/2} \qquad [32]$$

From Equation [17] or, what amounts to the same thing, a mass balance at each station s

$$\Psi = \frac{1}{1 + j}\rho_\infty U_\infty r^{1 + j} = \int_0^\delta r^j \rho\, u\, dy \qquad [33]$$

In difference form

$$\Delta\Psi_i = \frac{1}{1 + j}\rho_\infty U_\infty\left(r_{b_i}^{1+j} - r_{b_{i-1}}^{1+j}\right) = r^j \rho\, u\, \Delta y$$

where

$$u = u_b + \frac{\Sigma\Delta\Psi_i}{\Psi_s}(u_s - u_b) \qquad @\ s = \text{constant}$$

will provide the corresponding variation of y and the shock layer thickness. The effects of radiation cooling on the shock layer temperature distribution can now be determined through the energy equation including the radiation term.

$$\frac{\partial}{\partial s}\left(\frac{S}{C_v}\right) = -\frac{4\,\alpha_p\,\sigma\,T^4}{\rho\, u\, C_v\, T} \qquad [22]$$

The entropy variation can be expressed as:

$$p/\rho^{\gamma} = \left(p_r/\rho_r^{\gamma}\right) e^{\frac{S-S_r}{C_v}} \quad \text{for} \quad \gamma \to 1 \Longrightarrow T \simeq T_r \, e^{\frac{S-S_r}{C_v}}$$

$$\therefore \frac{\partial}{\partial s}\left(\frac{S}{C_v}\right) = \frac{1}{T}\frac{\partial T}{\partial s}$$

and Equation [22] becomes:

$$\frac{\partial T}{\partial s} = - \frac{4 \alpha_p \sigma T^4}{\rho u C_v} \qquad [34]$$

The absorption coefficient can be expressed as:

$$\alpha_p = \bar{\alpha}_p \rho^a T^b$$

where a and b are determined from opacity data (a = 1, b = 5, accurate for $T \leq 15{,}000$ deg K; see Reference 10). The energy equation becomes then:

$$\frac{\partial T}{\partial s} = - \frac{4 \bar{\alpha}_p \sigma T^{4+b}}{u C_v}$$

Separating the variables and integrating results in

$$\frac{T(s, s_s)}{T(s_s)} = \left[1 + 4 (3 + b) \frac{\bar{\alpha}_p \sigma}{C_v} \left[T(s_s)\right]^{3+b} \int_{s_s}^{s} \frac{ds}{u}\right]^{-\frac{1}{3+b}} \qquad [35]$$

where the subscripted variable s_s again refers to the entry point of a particular streamline into the shock layer. From the form of Equation [35], the temperature reduction (radiative cooling effect) along a particular streamline is seen to be greatest along those streamlines closest to the body surface. This is so because these streamlines enter the shock layer in the stagnation region where the temperature $T(s_s)$ is greatest and the velocity is lowest.

4. Radiative Heating. With the temperature distribution throughout the shock layer available, it is now possible to determine the radiation heating level to the body.

From:

$$\frac{\partial q_r}{\partial y} = 2\ \alpha_p\ \sigma\ T^4$$

applying the transformation (Equation [18b])

$$r^j\ \rho\ u\ \frac{\partial q_r}{\partial \Psi} = 2\ \alpha_p\ \sigma\ T^4$$

or

$$q_r = \int_o^{\Psi} 2\ \frac{\alpha_p\ \sigma\ T^4}{r^j\ \rho\ u}\ d\Psi$$

utilizing $\alpha_p = \bar{\alpha}_p\ \rho^a\ T^b$ and $d\Psi = \rho_\infty\ U_\infty\ r_b^j\ Z\ ds$

results in:

$$q_r = 2\ \bar{\alpha}_p\ \sigma\ \rho_\infty\ U_\infty\ \bar{r}_b \int_o^s \frac{Z\ T^{4+b}}{u}\ ds \qquad [36]$$

As with convection heating, we are interested in determining the total radiative heating to the body. Therefore:

$$Q_r = (2\pi)^j\ \bar{r}_b^{1+j} \int_o^s r^j\ q_r\ ds$$

$$= 2\ \bar{r}_b^{2+j}\ (2\pi)^j\ \bar{\alpha}_p\ \sigma\ \rho_\infty\ U_\infty\ T_t^{4+b} \int_o^s r^j \left[\int_o^s \frac{Z\ (T/T_t)^{4+b}}{u}\ ds \right] ds$$

Finally

$$\dot{r} \equiv \frac{d}{ds}\left[\frac{Q_r}{2(2\pi)^j\ \bar{\alpha}_p \sigma\ \rho_\infty\ \bar{r}_b^{2+j}\ T_t^{4+b}}\right] = r^j\ \lambda \qquad [37]$$

where

$$\dot{\lambda} = \frac{Z\ \bar{T}^{4+b}}{\bar{u}} \qquad [38]$$

and we have introduced:

$$\bar{T} = \frac{1}{\delta}\int_0^\delta \left(\frac{T}{T_t}\right) dy \quad \text{and} \quad \bar{u} = \frac{1}{\delta}\int_0^\delta \left(u/U_\infty\right) dy \qquad [39]$$

Treating the radiation terms in this manner, that is, taking mean values of temperature and velocity at a given station, amounts to treating the radiation as a distribution of sources along the shock layer.

The introduction of the total temperature T_t into Equation [37], together with the previously mentioned dimensionless coordinates, produces a dimensionless energy term just as in Equations [2] and [7]. (Equation [7]) is seen to be in terms of energy by multiplying the numerator and denominator of the left-hand side by the freestream velocity U_∞. It remains to relate the various energy terms through a common denominator.

PARAMETERS RELATING ENERGY FORMS

The energy levels of convective heating, radiative heating, and the work done by pressure drag will, of course, vary with Mach number and altitude. This will be accounted for by introducing the parameters

$$N_\alpha = \frac{\left[(\rho_e\ \mu_e)_o\right]^{1/2}\ U_\infty^{\frac{5}{2}}}{\bar{r}_b^{1/2}\ \rho_\infty\ U_\infty^3} \qquad [40]$$

and

$$N_\Gamma = \frac{\bar{\alpha}_p \sigma \rho_\infty \bar{r}_b T_t^{4+b}}{\rho_\infty U_\infty^3} \qquad [41]$$

into the right-hand sides of Equations [2] (and/or Equation [5]) and Equation [38], thus relating the energy forms to the common freestream energy. The Mach number and altitude variance of the parameters N_α and N_Γ, representative of the flight corridor as shown in Figure 4, are provided in Table 1. From here it is seen that the level of convection and radiation is considerably less than the work related to pressure drag (which is directly proportional to the freestream energy $\rho_\infty U_\infty^3$) for much of the flight corridor, becoming significant in a relative sense at the higher Mach numbers and altitudes (in the Mach number range beyond that of Table 1, the radiative heating would become dominant).

The necessary first-order differential equations for the Mayer problem formulation of the minimum energy body shapes can now be summarized as:

$$\dot{\alpha} = N_\alpha (u/U_\infty) Z^2 r^{2j}/\eta^{1/2} \qquad [42]$$

$$\dot{\eta} = (u/U_\infty) Z^2 r^{2j} \qquad [43]$$

$$\dot{\beta} = Z^3 r^j \qquad [44]$$

$$\dot{\Gamma} = r^j \lambda \qquad [45]$$

$$\dot{\lambda} = N_\Gamma \frac{Z \bar{T}^{4+b}}{\bar{u}} \qquad [46]$$

$$\dot{x} = (1 - Z^2)^{1/2} \qquad [47]$$

$$\dot{r} = Z \qquad [48]$$

where (u/U_∞) is provided by Equation [28] and x and y have been added to account for the body shape itself. $\bar{T}$ and $\bar{u}$ are obtained from Equation [39] after Equations [28], [30] through [33], and [35] have been solved to provide the shock layer properties.

A numerical application of the maximum principle to the above equations will produce the desired optimum shapes. A brief discussion of this principle is in order.

THE PONTRYAGIN MAXIMUM PRINCIPLE

The maximum principle serves to minimize some quantity:

$$J = \phi\ (x^f\ ,\ t^f) \qquad [49]$$

subject to the differential constraints

$$\dot{x}_i = f_i\ (x,\ u) \quad i = 1,\ n \qquad [50]$$

the boundary conditions

$$x = x^o \quad @ \quad t = t^o \qquad [51]$$

and end constraints

$$\Psi_j\ (x^f\ ,\ t^f) = 0 \quad j = 1,\ m \quad m < n$$

The variables x_i are referred to as state variables, u is the control variable (or variables), and t is the independent variable. In this context, the superscripts o and f refer to initial and final values, respectively (i.e., initial and final in the range $t^o \leq t \leq t^f$).

To apply the principle, it is necessary to introduce the adjoint variables obtained by

$$\dot{P}_i = -\ P_j \frac{\partial f_j}{\partial x_i} \quad i = 1,\ n \qquad [52]$$

along with the transversality conditions

$$\begin{aligned} P_i + \mu_j \frac{\partial \Psi_j}{\partial x_i} + \frac{\partial \phi}{\partial x_i} &= 0 \\ & \qquad i = 1,\ n\ (t = t^f) \qquad [53] \\ P_i\ f_i = \mu_j \frac{\partial \Psi_j}{\partial t} + \frac{\partial \phi}{\partial t} & \end{aligned}$$

where μ_i are constants associated with the various end constraints,

and the Hamiltonian

$$H = P_i f_i = H (P, x, u)$$

(repeated subscripts imply summation).

A minimum of J is obtained when the optimum control u(t) is found which satisfies the condition

$$H (P, x, \tilde{u}) \geq H (P, x, u) \qquad [54]$$

at every point on the trajectory. The numerical means of attaining this condition will be the method of steepest descent or the gradient method. Reference 15 provides the details of both the maximum principle and the gradient method.

Basically the procedure involves the assumption of an optimum condition or, equivalently, an assumed control function u(t). Through the assumed control, the state variables $x_i(t)$ may be obtained by numerically integrating Equation [50] from the initial conditions x^o through $(x(t^f))$ while satisfying the constraints $\Psi_j(x^f, t^f)$. The adjoint variables are then obtained by integrating Equation [52] backwards, from t^f to t^o; the values of the adjoint variables at t^f are supplied by the transversality conditions (Equation [53]). The Hamiltonian can then be formed and through changes in the control variable by

$$\delta u_i = \frac{1}{2\nu} P_j \frac{\partial f_j}{\partial u_i} \qquad [55]$$

a new control can be determined such that $H (P, x, \tilde{u}) \geq H (P, x, u)$ where $\tilde{u} = u + \delta u$.

On obtaining the closer to the optimum control u(t), a new family of state $x_i(t)$ and adjoint $P_i(t)$ variables is obtained. This procedure is repeated, adjusting the constants μ_j in Equation [53] to satisfy the end constraints until the condition of Equation [54] is satisfied throughout the range $t^o \leq t \leq t^f$ or, equivalently, the gradient of Equation [55] goes to zero, at which point the minimum values of [49] will be reached.

In the present problem, the independent variable is the arc length s and the state variables are $\alpha(s)$, $\eta(s)$, $\beta(s)$, $\Gamma(s)$, $\lambda(s)$, x(s), and r(s). The control variable is the local body slope Z(s). The differential

constraints are accordingly Equations [42] through [48]. The nose shapes being considered must maintain a given fineness ratio. By stopping the numerical integration at a predetermined x value, it is necessary to impose only a single end constraint to maintain the desired fineness ratio, i.e.,

$$\Psi_1 \left[r(s_f)\right] = r_f - 1 = 0 \qquad [56]$$

Applying Equation [52], the differential adjoint equations are:

$$\dot{P}_1 = 0 \qquad [57]$$

$$\dot{P}_2 = P_1 \, (u/U_\infty) \, Z^2 \, r^{2j}/2\eta^{\frac{3}{2}} \qquad [58]$$

$$\dot{P}_3 = 0 \qquad [59]$$

$$\dot{P}_4 = 0 \qquad [60]$$

$$\dot{P}_5 = - P_4 \, r^j \qquad [61]$$

$$\dot{P}_6 = 0 \qquad [62]$$

$$\dot{P}_7 = -P_1 \, N_\alpha \, 2j \, (u/U_\infty) Z^2 \, r/\eta^{1/2} - P_2 \, 2j (u/U_\infty) Z^2 \, r - j \, P_3 \, Z^3 - j \, P_4 \, \lambda \qquad [63]$$

The quantities to be minimized, either alone or summed with another, are $\alpha(s_f)$, $\beta(s_f)$, and $\Gamma(s_f)$. Accordingly, $P_1(s_f)$, $P_3(s_f)$, and $P_4(s_f)$ are either -1.0 or 0.0, in accordance with Equation [53] and the condition for which the body shape is being optimized. Table 2 lists the appropriate values for the various optimum bodies being considered.

We obtain further from Equation [53]

$$P_2(s_f) = P_5(s_f) = P_6 = 0 \qquad [64]$$

Here $p_7(s_f) = -\mu_1$ where μ_1 is an undetermined constant that must be determined to satisfy the end constraint (Equation [56]).

The initial assumed optimum shape is that of a blunted cone; see Figure 5. The associated control variable Z(s), the initial conditions $\alpha(s_o) = \beta(s_o) = \Gamma(s_o) = \lambda(s_o) = x(s_o) = r(s_o) = 0$, $\eta(s_o) = \eta_o \neq 0$ (η_o obtained by applying the L'Hospital rule to the integral of Equation [42]

under the condition $s \to o$), and Equations [42] through [48] will then provide the family of state variables through the range $o \leq s \leq s_f$. Choosing the appropriate values of $P_1(s_f)$, $P_3(s_f)$, and $P_4(s_f)$ from Table 2, together with conditions of Equation [64], Equations [57] through [63] are integrated backwards, from $s = s_f$ to $s = o$, to obtain the family of adjoint variables $P_i(s)$. Variations in the control variable are then obtained through Equation [55] together with Equations [42] through [48] to provide:

$$\delta Z = \frac{1}{2\nu}\left[\left(P_1/\eta^{1/2} + P_2\right)\left(2\,(u/U_\infty)Zr^{2j}/\eta^{1/2} - 2\left(\frac{\gamma-1}{\gamma+1}\right)(u/U_\infty)^{-1}r^{2j}Z\,\frac{3\gamma-2}{\gamma}\right) + P_3\,3Z^2\,r^j + P_5\,\frac{\bar{T}}{\bar{u}}^{4+b} + P_7\right] \qquad [65]$$

(where ν is an arbitrary constant which helps to determine the control variation). Observing that the new control variable $\tilde{Z} = Z + \delta Z$ satisfies the condition of Equation [54] at every point in the range $o \leq s \leq s_f$, the control Z is replaced with $\tilde{Z}$ and a new family of state and control variables is generated. This procedure is repeated until further changes in the control fail to satisfy the maximum principle condition (Equation [54]).

When the optimum body shape being considered includes radiation effects, it is necessary to recalculate the shock layer properties (through Equations [28], [30] through [33], [35], and [39]) each time the body shape is changed through the adoption of a new control variable.

This sequence was programmed for the IBM 7090 and the minimum drag, minimum heat, and minimum energy nose shapes with a given fineness ratio were determined.

RESULTS AND DISCUSSION

SHOCK LAYER SOLUTION

The numerical procedure used to provide the shock layer temperature distribution was formulated to provide a solution that is both direct and rapid. These criteria are essential when it is realized that the shock layer properties must be recalculated after each iteration which determines a new shape closer to the optimum. Despite its simplicity, the method

shows reasonably good agreement with some of the more detailed numerical shock layer solutions. Figure 6 compares present results with those obtained by Zlotnick and Neumann as published in Reference 11. The numerical scheme in their solution was indirect; the shock shape was assumed and integration proceeded from shock to body. The greatest discrepancy between the methods is seen to be in the surface pressure distribution. The surface pressure obtained by the Zlotnick and Neumann method falls below that predicted by the Newtonian plus centrifugal, or Newton-Busemann pressure relation, which, in turn, is known to underestimate the pressure on a spherical body and leads to a fictitious free layer (negative pressure coefficient) beyond approximately the 60-degree position on the sphere. The modified Newtonian pressure relation used in the present method is known to correlate very well with experiment on bodies of this sort. This being so, the surface pressure distribution as shown by the Zlotnick-Newmann method should be somewhat higher with a resulting even closer correlation between the surface velocity and shock layer profiles.

The radiation cooling effect on the shock layer temperature distribution is shown in Figure 7. The rapid temperature drop just inside the shock is seen to emulate the cooling effect shown by the more detailed numerical solution of Cheng and Vincenti.[16]

OPTIMUM SHAPES

The numerical results of the optimization procedure were in agreement with previous experience in dealing with the axisymmetric minimum drag and minimum convective heat transfer bodies (Figures 8a and 8b). (From Figure 8 on, figures in this report were plotted directly by a General Dynamics SC 4020 using the computer output). The given fineness ratio minimum drag body is found to closely coincide with the 3/4 power law body predicted by direct application of the calculus of variations. The nose shape producing a minimum in convective heating is found to be flat faced, as in References 5 and 6, but with a less sharp corner than that obtained by Aihara (Reference 6) using the calculus of variations. (Although the flow field analysis of the present study was not detailed enough to account for such factors as separation and secondary shocks resulting from

overexpansion, it does appear that the rounded corner is more desirable since it is less likely to produce such flow conditions and the associated local hot spots.)

The optimum nose shape producing a minimum in radiative heating (Figure 8c) is found to be conical in shape as predicted by a number of authors (e.g., Reference 12). There is, however, a significant difference in that the conical tip is found to be cusp shaped. Such a tip may be impractical from a materials viewpoint, but it is a justifiable result from a gas dynamics point of view. The reasoning leading to the conical shape follows from the fact that a cone will avoid the high shock layer temperatures and entropy layer associated with the normal or near-normal shock of the blunt body. The cusped tip carries this reasoning a step further since such a shape would result in a slightly more oblique shock than the pure cone, thereby giving lower shock layer temperatures and less radiative heating to the body.

Table 3 shows the numerical values of the different variables for the various optimum shapes. (Because of the considerable increase in computing time when determining the radiation effect, through Γ_f, this variable was not determined in those cases where it was not being considered in the optimization process). The value of the parameters N_α and N_Γ is of little consequence in the resulting configuration when a single variable is being minimized. Thus, the values of α_f and Γ_f are not representative of a particular flight condition but simply provide a reference in the first three cases of Table 3 to show the effect on one variable while minimizing another. It is apparent that the drag level is considerably more sensitive to shape changes than is convective heating.

As stated earlier, the minimum energy nose shapes must be considered in a different light from the optimum shapes wherein a single quantity is being minimized. Specific freestream conditions must be considered here. However, before we proceed to specific conditions, it may be of interest to observe the effect of the various energy forms on the minimum energy shapes by assuming them to be of equal significance. This can be accomplished by letting $N_\alpha = N_\Gamma = 1.0$ in the optimization procedure. Figure 9a shows the resulting minimum energy shape when considering the sum of convection

heating and drag. The compromise is obvious in that the extent of the bluntness is reduced, as opposed to the minimum convective heating profile, falling between it and the minimum drag shape. Table 3 shows the increase in both α_f and Γ_f over those of their respective optimum shapes. Figures 9b and 9c together with Table 3, show the diminishing influence of convection on the minimum energy shape as N_α decreases to the levels associated with the actual flight corridor of Figure 4 (see Table 1). It is apparent that the minimum energy shape is fast approaching that of the minimum drag profile.

The effect of radiation on the minimum energy shape is shown in Figure 10. Figure 10a, obtained while giving the various energy terms equal weight by allowing $N_\alpha = N_\Gamma = 1.0$, shows the tendency toward the conical shape as discussed with regard to the minimum radiative heat transfer body. When more realistic values of N_α and N_Γ are considered, the profile (Figure 10b) approaches that of the minimum energy shapes, with an equivalent N_α, wherein radiation was not considered (Figure 9b). The profiles are found to be identical except at the tip, where the flat portion of the minimum energy shape, without considering radiation, has been replaced with a conical tip. Table 3 shows a slight reduction in drag, with a negligible penalty in convection, when including the effects of radiation (Cases 5 and 8).

The minimum energy concept considered to this point (i.e., what might be considered for the nose shape of a hypersonic cruise vehicle) would appear to lose significance below a Mach number of about 20. Below this range, the drag levels are such as to prevail in determining the minimum energy shape. A more suitable approach in the lower Mach number range would be to specify the heat load one could tolerate and then by maintaining α_f at some given value determined from the specified heat load, to minimize the drag variable β_f. It seems certain that the resulting configurations would fall between the minimum energy nose shape of Figure 9c and the optimum shape considering convection alone (Figure 8b); radiation would of course not be considered in this Mach number range. That is, the extent of the flat-faced portion would depend on the expected heat load, with the contour following a power law variation from there to the base.

The minimum energy nose shape considering convection and radiation simultaneously would be pertinent to a reentry body wherein these heating forms would be of near equal magnitude. Such conditions would exist in the vicinity of Mach 30, i.e., in the slightly superorbital speed range. In this case, the parameters N_α and N_Γ would be nearly equal and may be taken as unity. The freestream conditions and Mach number are those at 250,000 feet and $M_\infty = 30$.

Figure 11 shows the resulting nose shape and Case 10 of Table 3 the related numerical results. The now familiar conical tip is again in evidence; the considerable heftiness of the nose shape is undoubtedly a result of attempting to maintain some bluntness as relief for the convective heating. A comparison of Figures 11 and 10a (where convection, radiation, and drag were considered) shows a similarity between the two and emphasizes the slenderizing effect of including the drag. In all cases where it is considered, the concession to the radiation effect is concentrated near the tip and is simply to create as slender a cone as the given case will allow, ranging from the rather blunt cone of Case 10 (Figure 11) to the cusp tipped cone of Case 3 (Figure 8c).

The two-dimensional optimum nose shapes are shown beginning with Figure 12 with the related numerical values of the essential variables in Table 4. The minimum drag shape, Figure 12a, is that of a wedge and, as in the axisymmetric case, is in agreement with what has been shown by direct application of the calculus of variations.[17] The minimum heat transfer shape (convection) for the two-dimensional case, Figure 12b, is found to be flat faced, as in the axisymmetric case, but with a less extensive expanse of flatness (Figure 8b). This is significant when considered with the numerical values of Table 4. In going from the minimum drag shape of Case 11 to the minimum heat transfer shape of Case 12, the reduction in α_f is seen to be on the order of 10 percent while the drag level has increased by better than 50 percent. It is evident then that the drag variation is even more sensitive to shape changes than was the case with the axisymmetric bodies. This being so, the minimum energy shapes are dominated by the drag terms and, as can be seen in Cases 13 and 14 of Table 4, the convective and radiative heating have little effect on the numerical values. For all practical purposes, the two-dimensional

minimum energy shapes considering (1) convection and drag or (2) convection, radiation and drag were wedge shaped as already shown in Figure 12a. However Figure 13 is included to show the minimum energy shape for all three energy forms; with care, it is possible to detect a slight convex curvature in this figure.

CONCLUSIONS

The optimum hypersonic nose and leading edge shapes with a given fineness or thickness ratio were determined for a variety of optimizing criteria. The axisymmetric cases produced a near 3/4 power law profile for the minimum drag shape and a flat-faced nose for the minimum heat transfer considering convection alone. When both convection and drag were considered, the minimum energy nose shapes were flat faced but with a less extensive expanse of flatness than the minimum heat transfer noses. The influence of drag on the minimum energy shape was dominant at moderate hypersonic Mach numbers, suggesting an alternative approach at the lower Mach numbers, namely, specifying a given heat load and minimizing the drag. The results of this study indicate that such an approach would lead to similar flat-faced shapes with the expanse of flatness depending on the specified heat load.

When only radiation was considered, the optimum nose shape was conical with a cusped tip, the cusped tip being an apparent attempt to produce a more oblique shock than the pure cone and therefore lower shock layer temperatures.

When convection, radiation, and drag were considered the minimum energy nose shape was conical near the tip; the influence of radiation on the minimum energy shape was negligible except at the extreme Mach numbers that could be considered for a cruise vehicle (i.e., $20 \leq M \leq 25$).

When only convection and radiation were considered the minimum energy nose shape had a large angle conical tip. The conical tip provides relief from the severity of radiation and the blunting is retained to contend with convection.

The overall results clearly illustrate the geometric means of alleviating the various energy forms. Drag reduction is produced by a

slight degree of blunting near the tip, thereby reducing the body slope and therefore the pressure farther back on the body where the projected area (projected in the direction of the flight path) is greater. The effect of radiation is concentrated near the tip where the tendency is toward a cone so as to relieve the shock layer temperatures. Convection tends toward the blunt body with its lower surface velocities and therefore lower shear.

The two-dimensional cases produced a wedge shape for the minimum drag profile and a flat face for the minimum heat transfer (convection). The extent of flatness on the minimum heat transfer shape is considerably less than in the corresponding axisymmetric case. The drag is most susceptible to shape changes and is found to dominate when considered with the other energy forms. The result is that the two-dimensional minimum energy profiles are nearly wedge shaped in all cases considered.

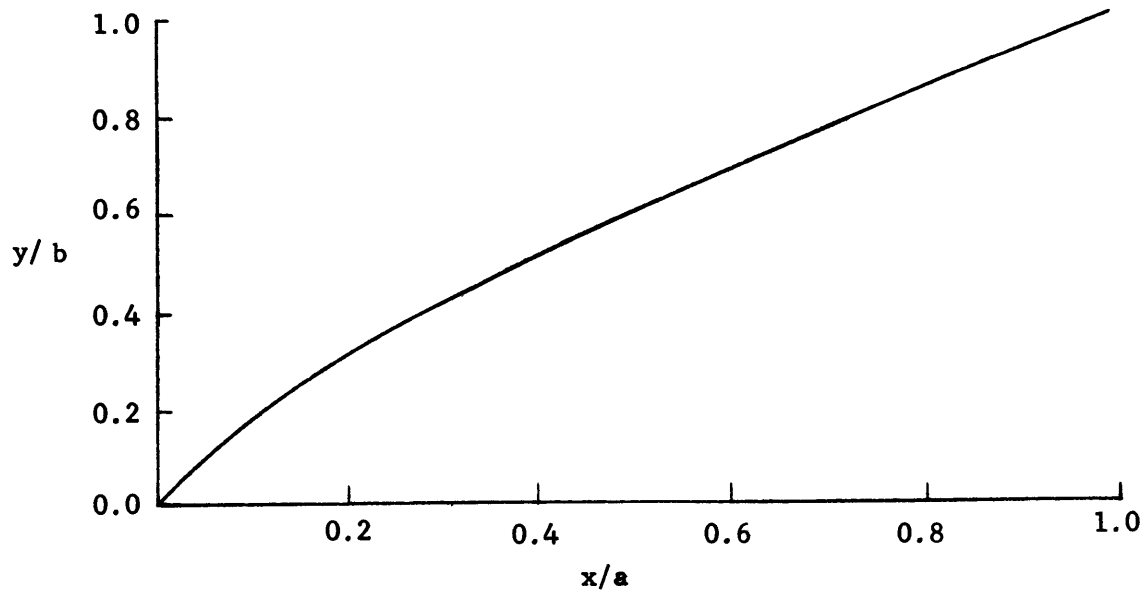

Figure 1a - Minimum Drag Body of Given Fineness Ratio (a/2b)

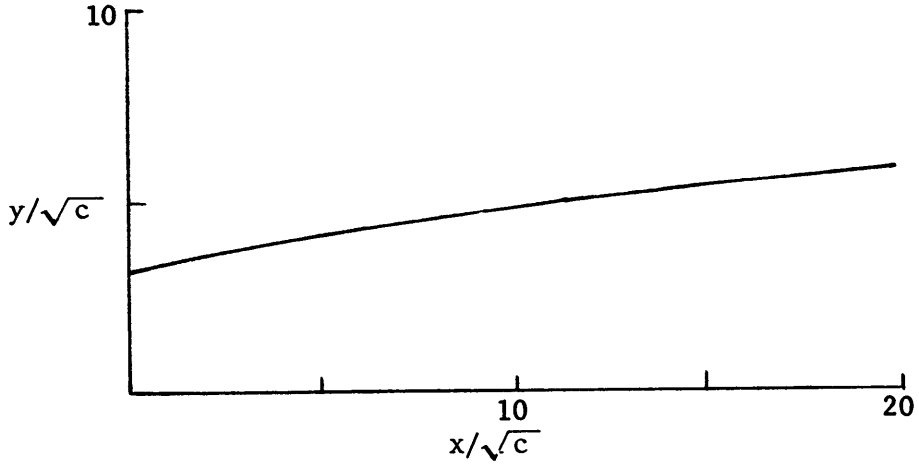

Figure 1b - Minimum Heat Transfer Body

Figure 1 - Optimum Hypersonic Nose Shapes

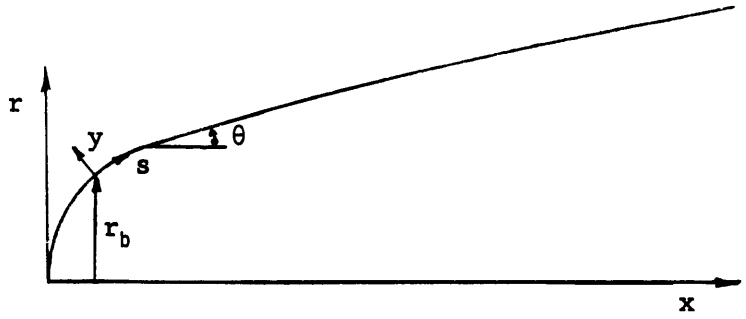

Figure 2 - Body-Oriented Coordinate System

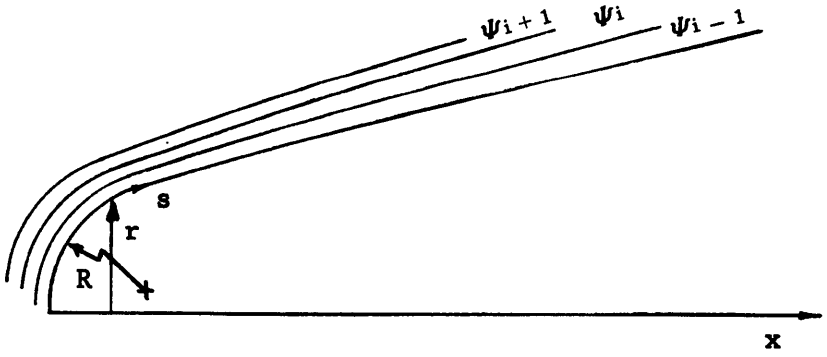

Figure 3 - Von Mises Coordinate System

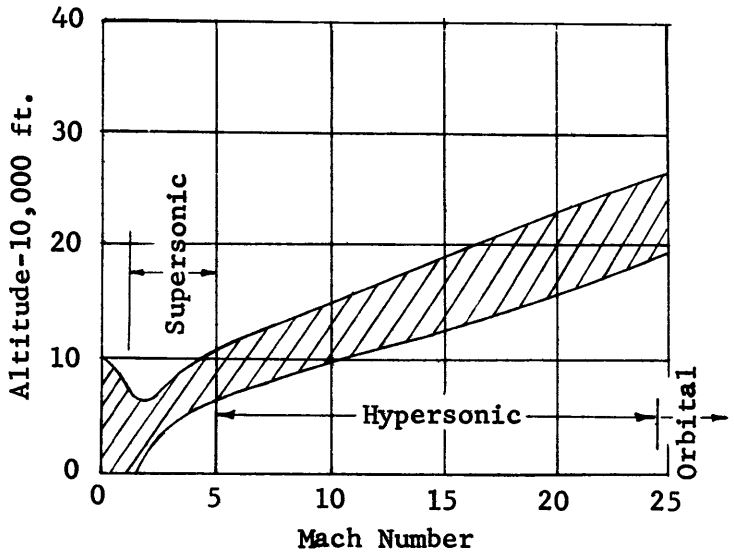

Figure 4 - Flight Corridor

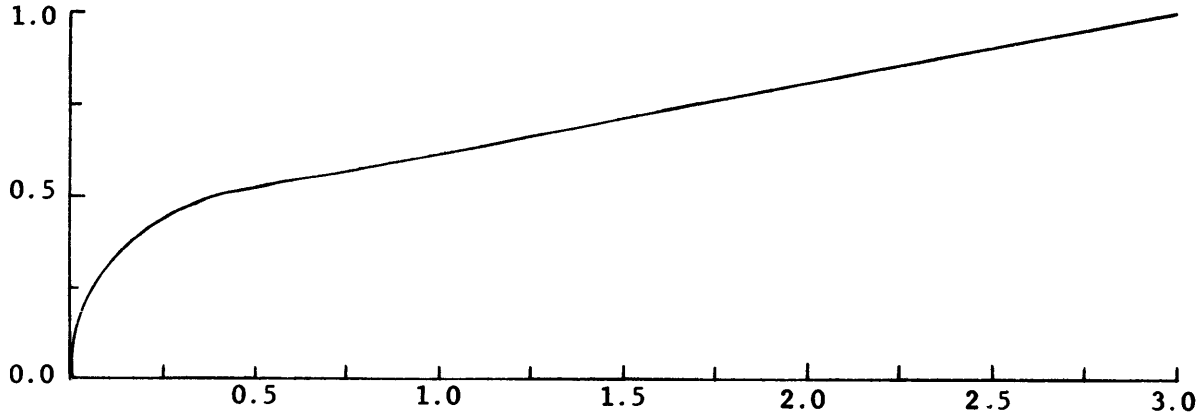

Figure 5 - Initial "Assumed" Optimum Shape

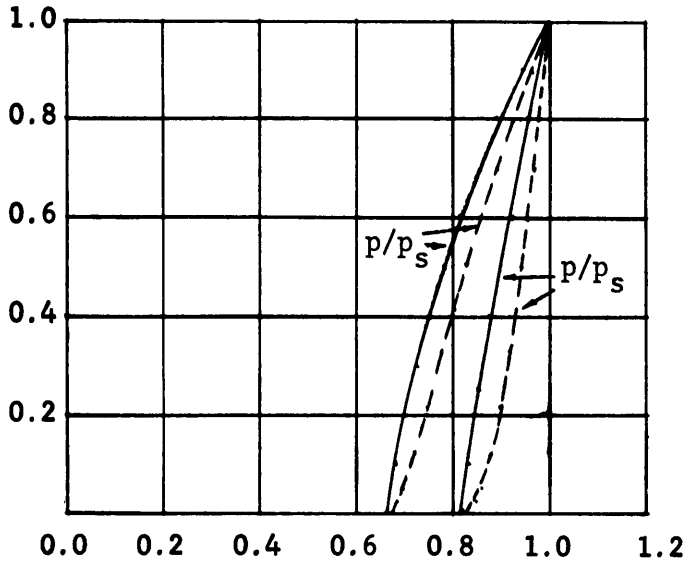

Figure 6a - Shock Layer Profiles
(θ = 32 Deg)

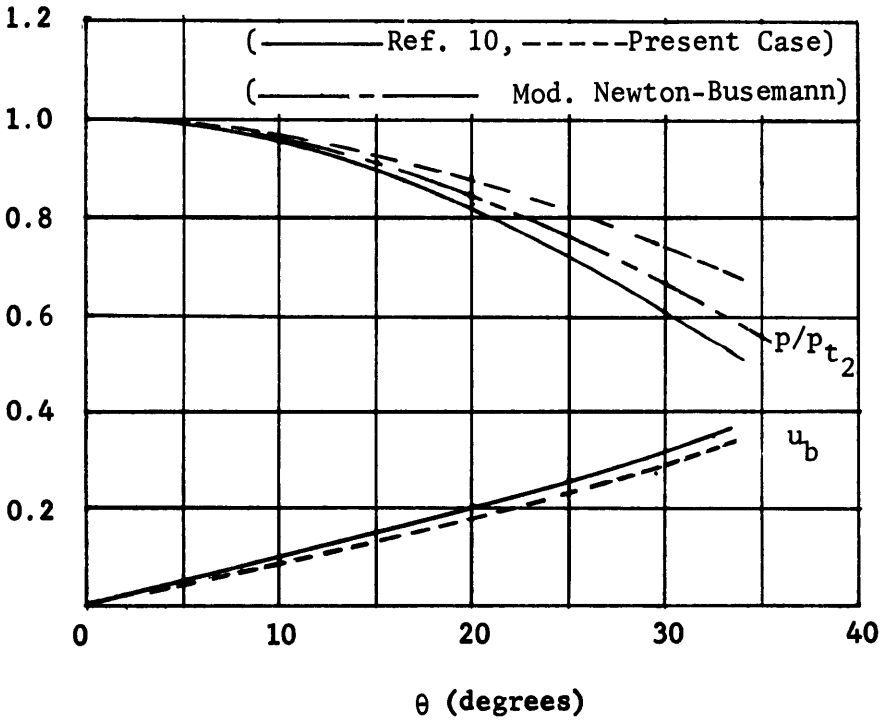

Figure 6b - Flow Variables at Body Surface

Figure 6 - Flow Properties for Spherical Body
γ = 1.2, M_∞ = 10

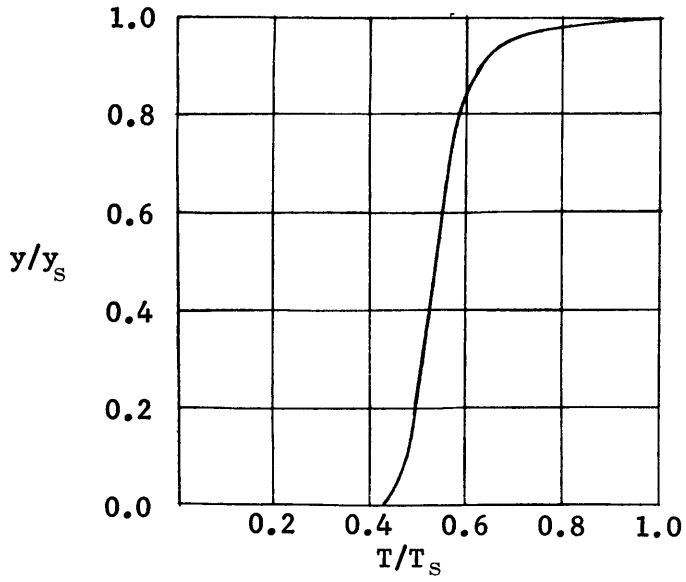

Figure 7a - Temperature Profile @ 60 from Stagnation Point on Hemispherical Nose

M = 50, Alt. = 100,000 ft.

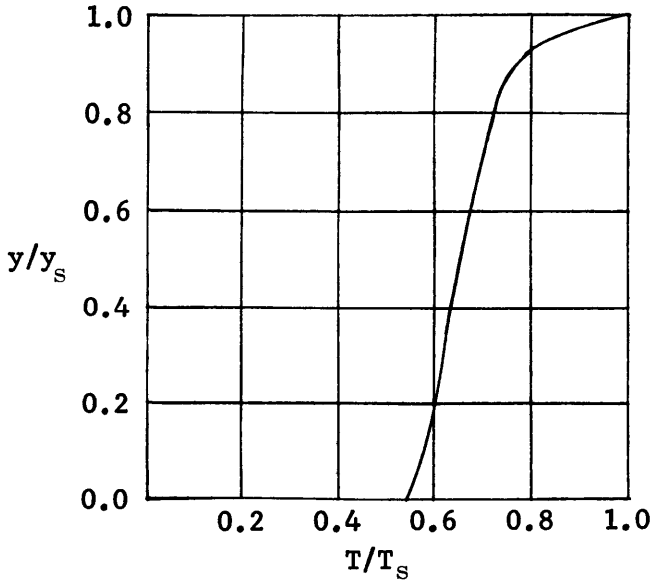

Figure 7b - Temperature Profile behind Parabaloidal Shock

Figure 7 - Radiative Cooling Effect on Shock Layer Temperature Distribution

Data are from Reference 16.

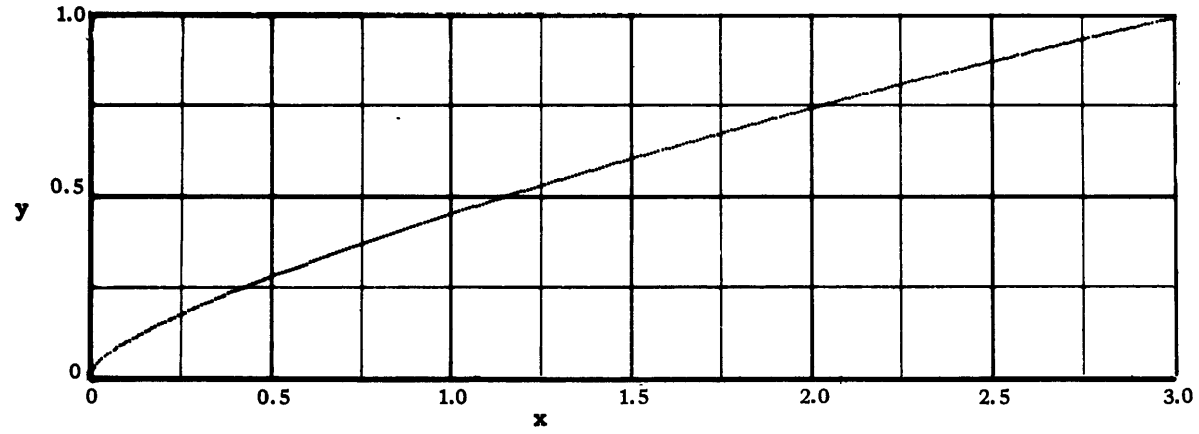

Figure 8a - Minimum Drag (Minimum β_f)

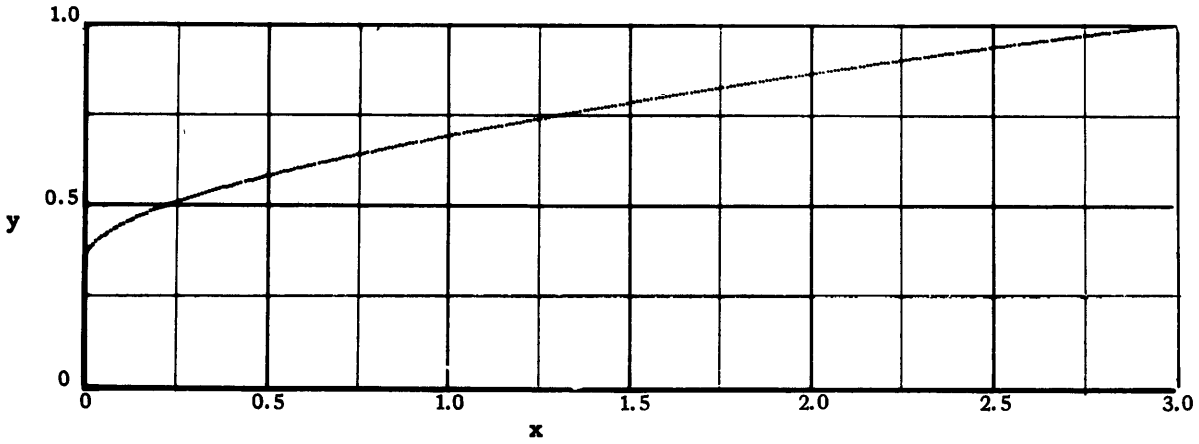

Figure 8b - Minimum Heat Transfer-Convection (Minimum α_f)

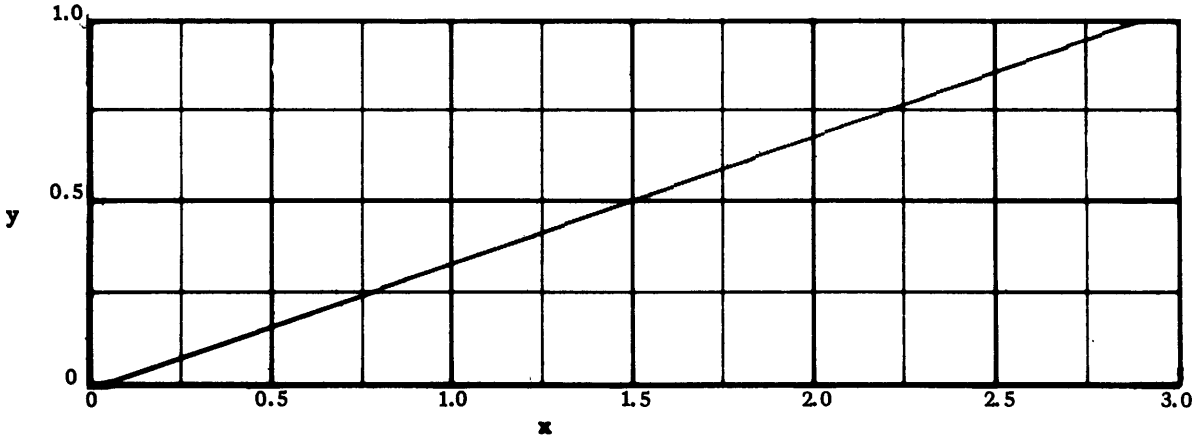

Figure 8c - Minimum Heat Transfer-Radiation (Minimum Γ_f)

Figure 8 - Optimum Nose Shapes - Axisymmetric (Fineness Ratio = 1.5)

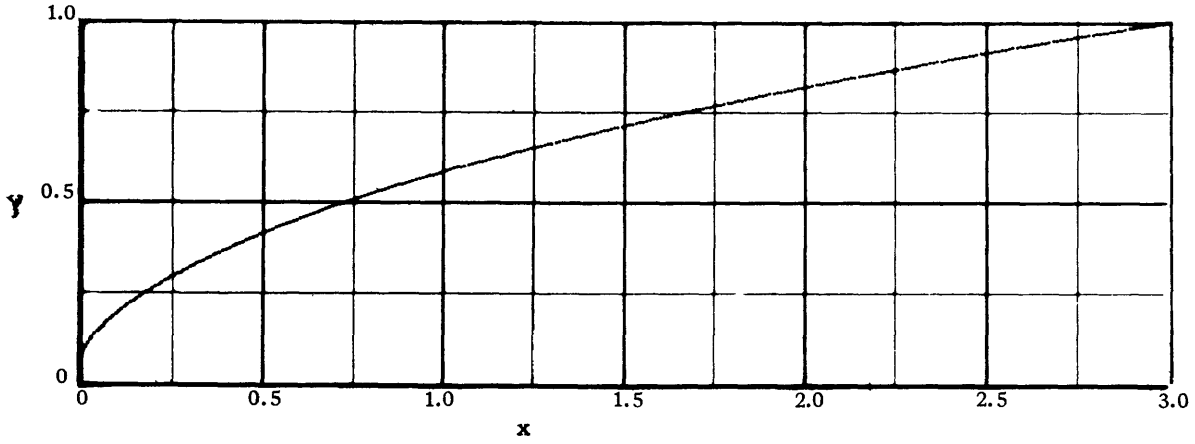

Figure 9a - Minimum $\alpha_f+\beta_f$ ($N_\alpha=1.0$)

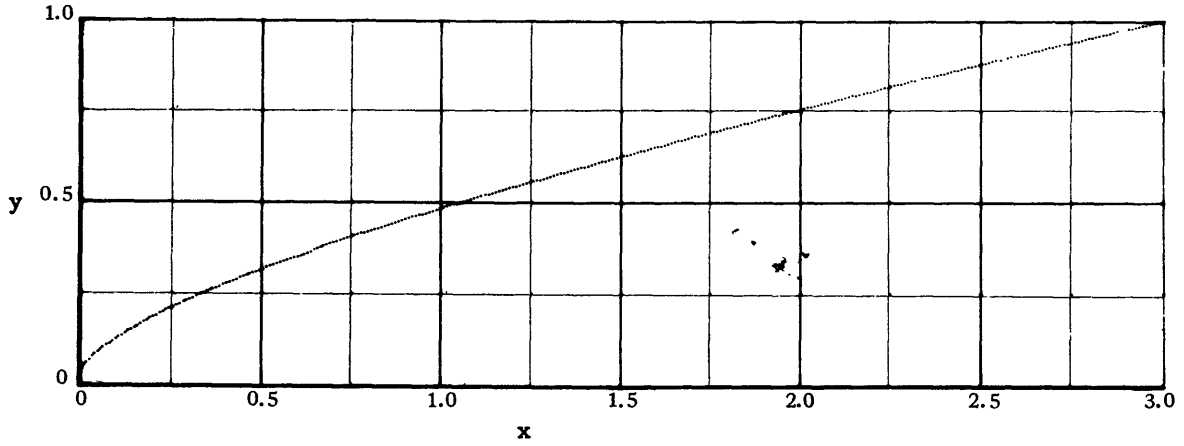

Figure 9b - Minimum $\alpha_f+\beta_f$ ($N_\alpha=0.1$)

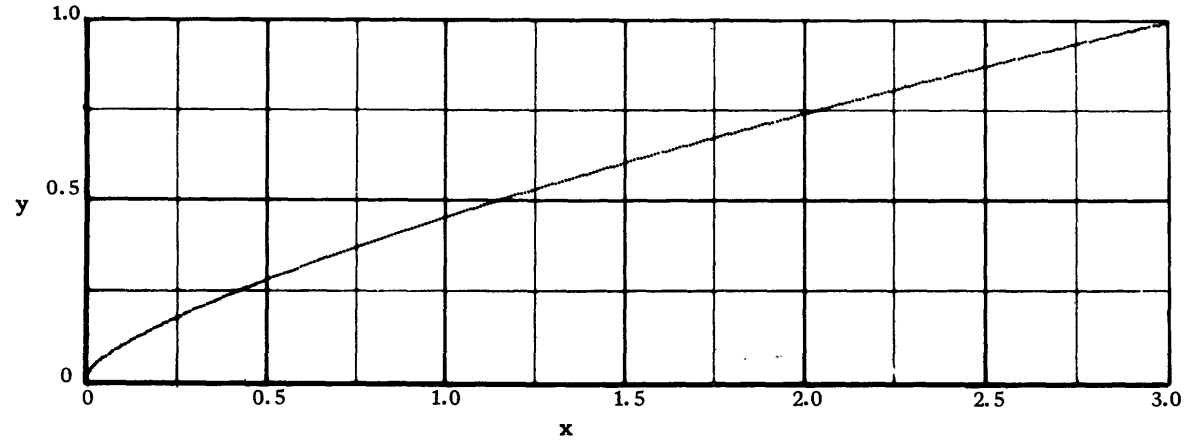

Figure 9c - Minimum $\alpha_f+\beta_f$ ($N_\alpha=0.1$)

Figure 9 - Minimum Energy Nose Shapes Considering Convection and Drag

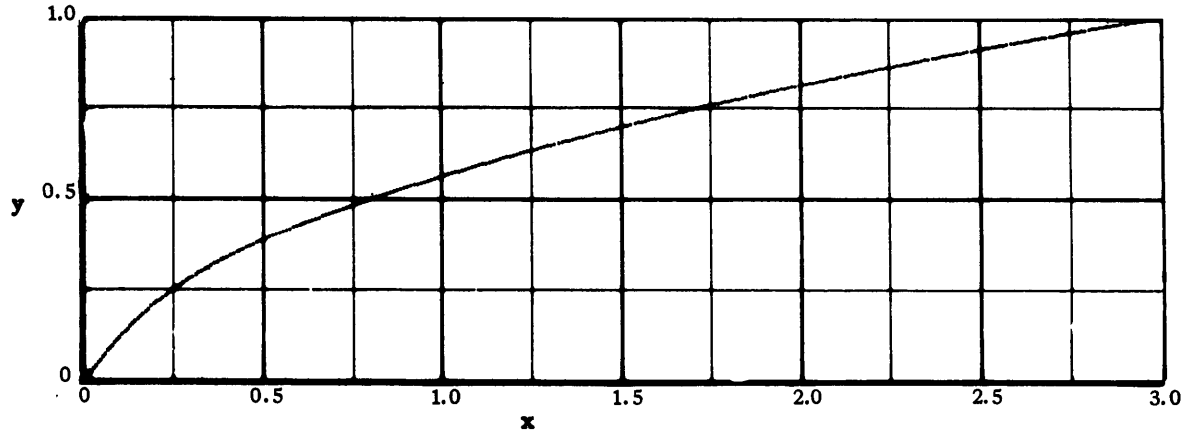

Figure 10a - Minimum $\alpha_f+\beta_f+\Gamma_f$ $(N_\alpha=N_\Gamma=1.0)$

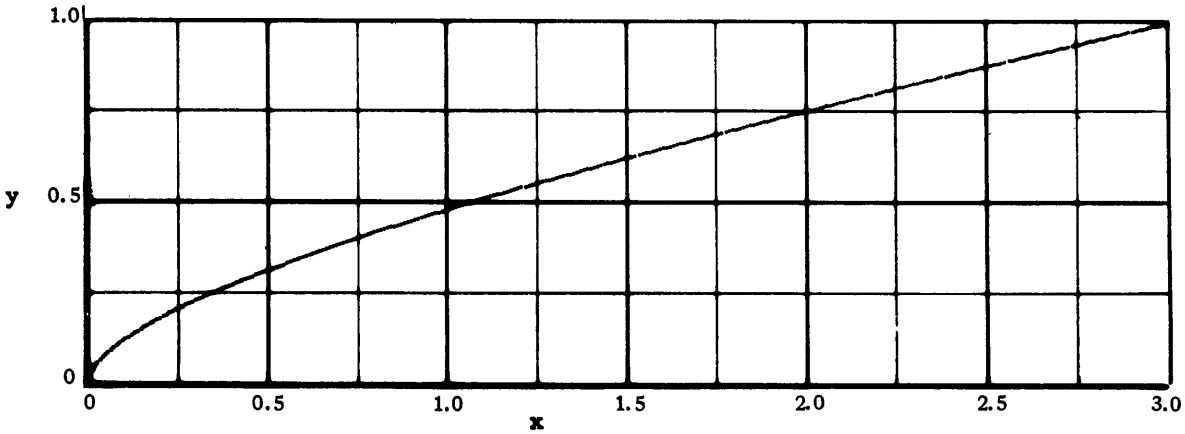

Figure 10b - Minimum $\alpha_f+\beta_f+\Gamma_f$ $(N_\alpha=0.1, N_\Gamma=0.01)$

Figure 10 - Minimum Energy Nose Shapes Considering Convection, Radiation, and Drag

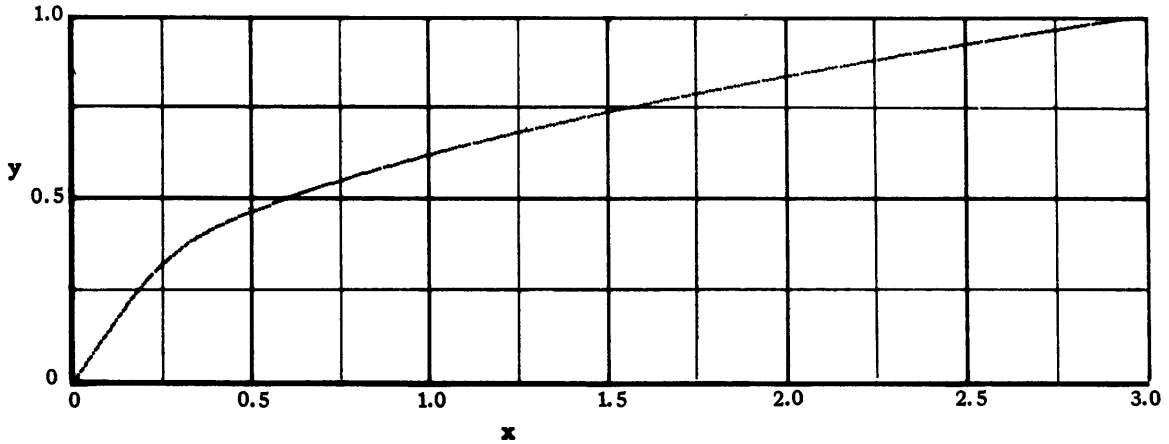

Figure 11 - Minimum Energy Considering Convection and Radiation (Minimum $\alpha_f+\Gamma_f$)

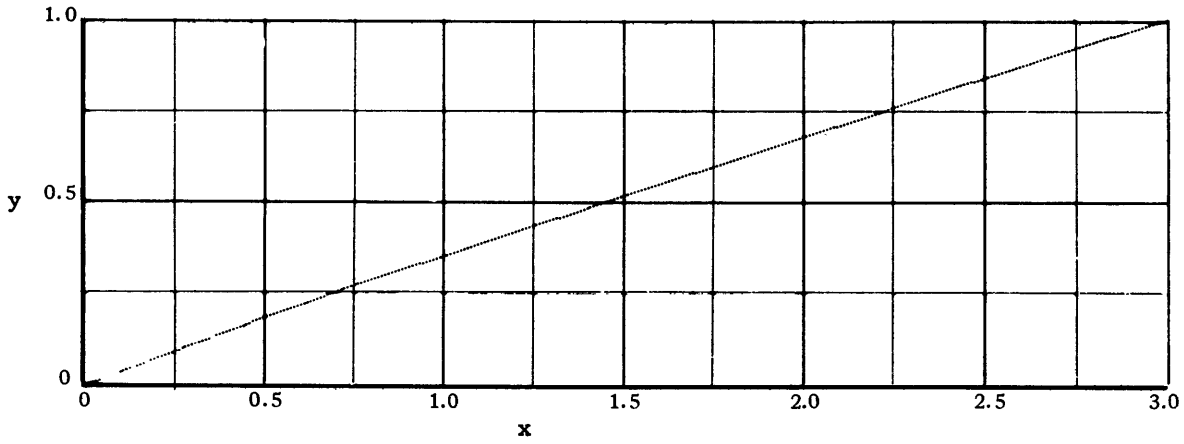

Figure 12a - Minimum Drag (Minimum β_f)

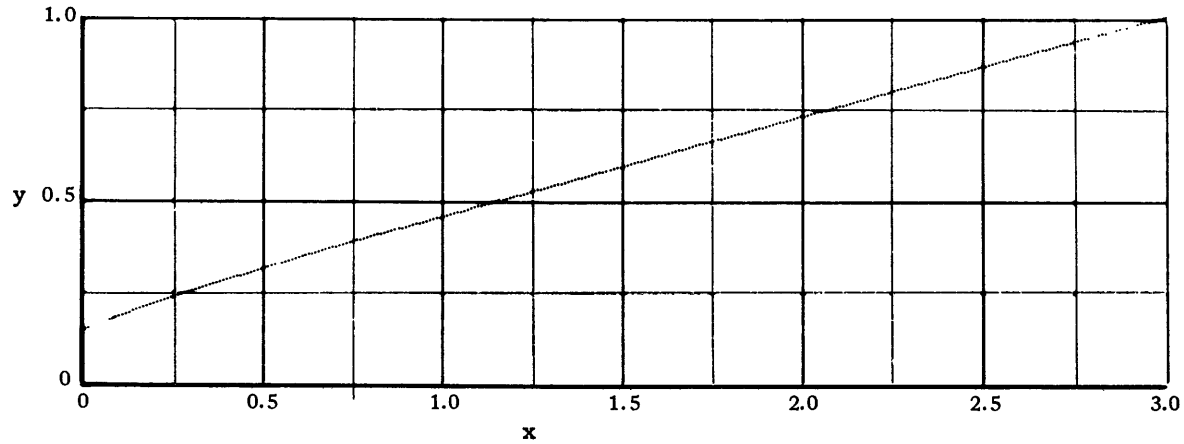

Figure 12b - Minimum Heat Transfer-Convection (Minimum α_f)

Figure 12 - Optimum Nose Shapes--Two-Dimensional (Fineness Ratio = 1.5)

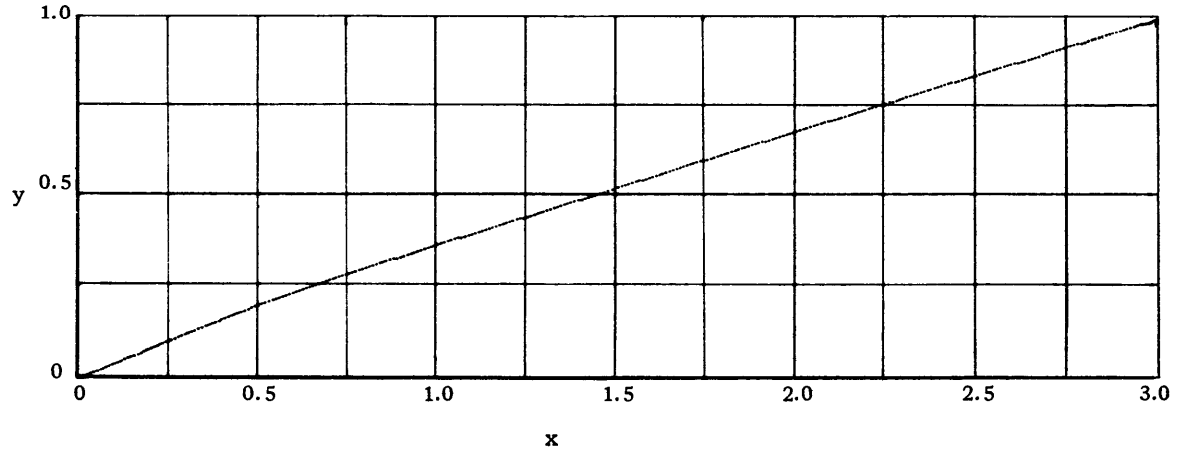

Figure 13 - Minimum Energy Leading Edge Shape Considering Convection, Radiation, and Drag (Minimum $\alpha_f + \beta_f + \Gamma_f$)

TABLE 1

Variation of Convective and Radiative Parameters with Mach Number and Altitude ($\gamma = 1.1$)

M_∞	Alt. x 10^{-3}	N_α x 10	N_Γ x 10
5	50	0.013	10^{-9}
	100	0.040	10^{-9}
10	100	0.016	
	150	0.054	
15	120	0.023	0.571×10^{-3}
	180	0.096	0.692×10^{-2}
20	150	0.061	0.181
	200	0.132	0.316
25	200	0.139	7.85
	250	0.288	0.728
30	200		109.6
	250		10.0

TABLE 2

Value of Adjoint Variables at $s = s_f$ for Various Optimum Shapes

Variable	ϕ	$P_1(s_f)$	$P_3(s_f)$	$P_4(s_f)$
Min. Drag	$\beta(s_f)$	0.0	-1.0	0.0
Min. Heat (Conv.)	$\alpha(s_f)$	-1.0	0.0	0.0
Min. Heat (Rad.)	$\Gamma(s_f)$	0.0	0.0	-1.0
Min. Energy (Conv. + Drag)	$\alpha(s_f)+\beta(s_f)$	-1.0	-1.0	0.0
Min. Energy (Conv. + Rad.)	$\alpha(s_f)+\Gamma(s_f)$	-1.0	0.0	-1.0
Min. Energy (Conv. + Rad. + Drag)	$\alpha(s_f)+\Gamma(s_f)+\beta(s_f)$	-1.0	-1.0	-1.0

TABLE 3

Convective, Radiative, and Drag Variables Related to Axially Symmetric Nose Shapes of Fineness Ratio 1.5

Case	Variable(s) Being Minimized	N_α	N_Γ	α_f	β_f	Γ_f
1	β_f	1.0	-	0.4310	0.0407	-
2	α_f	1.0	-	0.3880	0.0980	-
3	Γ_f	1.0	1.0	0.4720	0.0531	0.3×10^{-5}
4	$\alpha_f+\beta_f$	1.0	-	0.4200	0.0508	-
5	$\alpha_f+\beta_f$	0.1	-	0.1159	0.0420	-
6	$\alpha_f+\beta_f$	0.01	-	0.0836	0.0410	-
7	$\alpha_f+\beta_f+\Gamma_f$	1.0	1.0	0.4260	0.0505	0.0166
8	$\alpha_f+\beta_f+\Gamma_f$	0.1	0.01	0.1160	0.0410	0.3×10^{-3}
9	$\alpha_f+\Gamma_f$	1.0	1.0	0.4168	0.0651	0.0538

TABLE 4

Convective, Radiative, and Drag Variables Related to Two-Dimensional Leading Edge Shapes of Thickness Ratio 1.5

Case	Variable(s) Being Minimized	N_α	N_Γ	α_f	β_f	Γ_f
11	β_f	1.0	-	0.8040	0.1002	-
12	α_f	1.0	-	0.7182	0.2160	-
13	$\alpha_f+\beta_f+1.0$	1.0	1.0	0.8066	0.1027	-
14	$\alpha_f+\beta_f+\Gamma_f$	1.0	1.0	0.7952	0.0993	0.4×10^{-4}

REFERENCES

1. Miele, Angelo. The Calculus of Variations in Applied Aerodynamics and Flight Mechanics. [Seattle] Jun 1961. 105 p. illus. (Boeing Scientific Research Lab. D1-82-0113).

2. Eggers, Alfred, J., Jr. Meyer M. Resnikoff and David H. Dennis. Bodies of Revolution Having Minimum Drag at High Supersonic Airspeeds. Wash., 1957. 12 p. incl. illus. (National Advisory Committee for Aeronautics. Rpt. 1306. Supersedes TN 3666).

3. Allen, Harry J. and Alfred J. Eggers, Jr. A Study of the Motion and Aerodynamic Heating of Ballistic Missiles Entering the Earth's Atmosphere at High Supersonic Speeds. Wash., 1958. 16 p. incl. illus. (National Advisory Committee for Aeronautics. Rpt. 1381. Supersedes TN 4047).

4. Hanawalt, A.J., A.H. Blessing and C.M. Schmidt. Thermal Analysis of Stagnation Regions With Emphasis on Heat-Sustaining Nose Shapes at Hypersonic Speeds. Journal of the Aerospace Sciences (N.Y.), v. 26, May 1959, p. 257-263.

5. Furey, Roger J. Optimum Super/Hypersonic Leading-Edge Profiles. Wash., Jul 1965. 30 l. incl. illus. (Naval Ship Research and Development Center. Rpt. 2035. Aero Rpt. 1091) (DDC AD 471 674).

6. Aihara, Yasuhiko. Optimum Body Geometries of Minimum Heat Transfer at Hypersonic Speeds. AIAA Journal (N.Y.) v. 6, Nov 1968, p. 2187-2189.

7. Lees, Lester. Laminar Heat Transfer Over Blunt-Nosed Bodies at Hypersonic Flight Speeds. Jet Propulsion (N.Y.), v. 26, Apr 1956, p. 259-269.

8. Vincenti, Walter G. and Charles H. Kruger, Jr. Introduction to Physical Gas Dynamics. N.Y., Wiley [1965] 538 p.

9. Freeman, N.C. On the Theory of Hypersonic Flow Past Plane and Axially Symmetric Bluff Bodies. Journal of Fluid Mechanics (London), v. 1, Oct 1956, p. 366-387.

10. Wang, K.C. Radiating Shock Layers. Baltimore, Jun 1965. 61 p. incl. illus. (Martin Co. Research Rpt. 67).

11. Hayes, Wallace D. and Ronald F. Probstein. Hypersonic Flow Theory. Vol. 1: Inviscid Flows. [2d ed.] N.Y., Academic Press, 1966.

12. Hoshizaki, H. and K.H. Wilson. Viscous, Radiating Shock Layer About a Blunt Body. AIAA Journal (N.Y.) Sep 1965, p. 1614-1622.

13. Maslen, S.H. Inviscid Hypersonic Flow Past Smooth Symmetric Bodies. AIAA Journal (N.Y.), v. 2, Jun 1964, p. 1055-1061.

14. National Advisory Committee for Aeronautics. Equations, Tables, and Charts for Compressible Flow. Wash., 1953. 69 p. illus. (Rpt. 1135. Supersedes TN 1428).

15. McIntyre, J.E. Guidance, Flight Mechanics and Trajectory Optimization. Vol. 7: The Pontryagin Maximum Principle. Wash., Mar 1968. 126 p. incl. illus. (National Aeronautics and Space Adm. CR-1006) (North American Aviation, Inc. Rpt. SID 65-1200-7).

16. Cheng, Ping and Walter G. Vincenti. Inviscid Radiating Flow Over a Blunt Body. Journal of Fluid Mechanics (London), v. 27, Mar 1967, p. 625-646.

17. Chapman, Dean R. Airfoil Profiles for Minimum Pressure Drag at Supersonic Velocities. Wash., 1952. 14 p. incl. illus. (National Advisory Committee for Aeronautics. Rpt. 1063. Supersedes TN 2264).

INITIAL DISTRIBUTION

Copies	
1	Commander, Naval Ordnance Systems Command Headquarters Attn: NAVORD 035
7	Commander, Naval Air Systems Command Headquarters Attn: 1 NAVAIR 03B 1 NAVAIR 03C 1 NAVAIR 320 1 NAVAIR 320C 1 NAVAIR 310 2 NAVAIR 604
1	ONR, Attn: Mr. Morton Cooper ONR 430B
1	Commander, Naval Weapons Center Attn: Tech Lib (Code 753)
1	Dir, NRL Attn: Tech Lib
1	NASA, High Speed Flight Station, Edwards Air Force Base
3	NOL Attn: 1 Dr. John D. Anderson 1 Dr. Andrew H. Van Tuyl 1 Library
1	NASA, Ames Research Center Moffett Field, Calif Attn: Library
1	NASA, Headquarters, Wash., D.C. Attn: Chf., Div of Res Info
3	NASA, Langley Research Center Attn: 1 Comp. Res. Div 1 Theoretical Aerodynamics Div 1 Library
1	NASA, Lewis Research Center Cleveland, Ohio Attn: Lib
1	NASA, George C. Marshall Space Flight Center Attn: Tech Lib
2	Director, Defense Res & Engr Attn: 1 Mr. Branson Smith 1 Library
20	DDC

Copies	
1	Commander, Naval Missile Center, Pt. Magu Attn: Library
1	CO, USA Aberdeen Res & Development Center Attn: Tech Lib (STEAP-TL)
1	Commander, NWL Attn: Lib
1	Aerospace Research Labs, WPAFB Attn: Tech Lib
1	Headquarters, Arnold Engr Development Center Attn: Lib/Documents
1	Commanding General, U.S. Army Missile Command Attn: Chief, Document Section
1	Office of the Chief of Research & Development (ABMDA), Pentagon
1	Commander, Naval Air Development Center, Johnsville, Pa.
1	Commanding Officer, U.S. Air Force Weapons Lab, Kirtland Air Force Base Attn: WLRP
1	JHU, Applied Physics Lab Attn: Document Lib
1	Scientific & Technical Information Facility Attn: NASA Rep. (S-AK/DL)
1	George Washington Univ., School of Engr Attn: Dr. George Lea
1	Institute for Defense Analysis, Arlington, Va. Attn: Robert Oliver
3	Martin-Marietta Corp, Denver Div Attn: 2 Mr. Emmett Mossman 1 Lib

Copies

2 Hercules, Inc., Allegany
Ballistics Lab.
Attn: 1 Mr. W.T. Freeman
1 Lib

1 Rice Univ, School of Engr
Attn: Dr. Angelo Miele

UNCLASSIFIED

Security Classification

DOCUMENT CONTROL DATA - R & D

(Security classification of title, body of abstract and indexing annotation must be entered when the overall report is classified)

1 ORIGINATING ACTIVITY *(Corporate author)* Naval Ship Research and Development Center Washington, D.C. 20007	2a. REPORT SECURITY CLASSIFICATION Unclassified 2b. GROUP

3 REPORT TITLE

MINIMUM ENERGY HYPERSONIC NOSE AND LEADING EDGE SHAPES

4 DESCRIPTIVE NOTES *(Type of report and inclusive dates)*

5 AUTHOR(S) *(First name, middle initial, last name)*

Roger J. Furey

6 REPORT DATE September 1969	7a. TOTAL NO OF PAGES 49	7b. NO. OF REFS 17
8a. CONTRACT OR GRANT NO. b. PROJECT NO. WR 009 0201 c. Task 10204 d.	9a. ORIGINATOR'S REPORT NUMBER(S) 3186 9b. OTHER REPORT NO(S) *(Any other numbers that may be assigned this report)* Aero 1164	

10 DISTRIBUTION STATEMENT

This document has been approved for public release and sale; its distribution is unlimited.

11 SUPPLEMENTARY NOTES	12. SPONSORING MILITARY ACTIVITY Commander Naval Air Systems Command (NAVAIR 320) Washington, D.C. 20360

13. ABSTRACT

A system of first-order differential equations governing the heat transfer (convection and shock layer radiation) and pressure drag of an axisymmetric or two-dimensional body in hypersonic flow is developed. The Pontryagin Maximum Principle is applied to this system, through the gradient method, and a series of optimum hypersonic nose and two-dimensional shapes of given fineness ratio is found. The axisymmetric minimum drag shape is similar to the familiar 3/4 power law profile while the two-dimensional result is wedge shaped. The minimum heat transfer profiles are found to be flat faced when considering convection alone and conical, with a cusped tip, when considering radiation alone. Minimum energy shapes are found wherein the various energy terms being minimized include the sum of convection plus drag work, convection plus radiation plus drag work and convection plus radiation. The axisymmetric results show reasonable accommodation for the various energy forms considered in each of the minimum energy nose shapes. The two-dimensional minimum energy shapes are found to be dominated by the drag work with the results being, for all practical purposes, wedge shaped.

14 KEY WORDS	LINK A		LINK B		LINK C	
	ROLE	WT	ROLE	WT	ROLE	WT
Optimum Aerodynamic Shapes						
Minimum Drag						
Minimum Heat Transfer						
Minimum Energy Shapes						

Naval Ship R&D Center. Report 3186.
MINIMUM ENERGY HYPERSONIC NOSE AND LEADING EDGE SHAPES, by Roger J. Furey. Wash., Sep 1969. vi, 43p. illus., refs. (Aerodynamics Laboratory. Aero Rpt. 1164. Aero Problem 648-240) (NASC Project WR 009 0201) UNCLASSIFIED

A system of first-order differential equations governing the heat transfer (convection and shock layer radiation) and pressure drag of an axisymmetric or two-dimensional body in hypersonic flow is developed. The Pontryagin Maximum Principle is applied to this system, through the gradient method, and a series of optimum hypersonic nose and two-dimensional shapes of given fineness ratio is found. The axisymmetric minimum drag shape is similar to the familiar 3/4 power law profile while the two-dimensional result is wedge shaped. The minimum

Drag, Minimum
Drag, Hypersonic
Heat Transfer, Minimum
Heat Transfer, Hypersonic
Heat Transfer--Bodies, Blunt
Heat Transfer--Bodies, Two-Dimensional
Heat Transfer--Bodies, Axisymmetric
Wings--Thickness, Leading Edge
Airplanes, Hypersonic--Design

Naval Ship R&D Center. Report 3186.
MINIMUM ENERGY HYPERSONIC NOSE AND LEADING EDGE SHAPES, by Roger J. Furey. Wash., Sep 1969. vi, 43p. illus., refs. (Aerodynamics Laboratory. Aero Rpt. 1164. Aero Problem 648-240) (NASC Project WR 009 0201) UNCLASSIFIED

A system of first-order differential equations governing the heat transfer (convection and shock layer radiation) and pressure drag of an axisymmetric or two-dimensional body in hypersonic flow is developed. The Pontryagin Maximum Principle is applied to this system, through the gradient method, and a series of optimum hypersonic nose and two-dimensional shapes of given fineness ratio is found. The axisymmetric minimum drag shape is similar to the familiar 3/4 power law profile while the two-dimensional result is wedge shaped. The minimum

Drag, Minimum
Drag, Hypersonic
Heat Transfer, Minimum
Heat Transfer, Hypersonic
Heat Transfer--Bodies, Blunt
Heat Transfer--Bodies, Two-Dimensional
Heat Transfer--Bodies, Axisymmetric
Wings--Thickness, Leading Edge
Airplanes, Hypersonic--Design

Naval Ship R&D Center. Report 3186.
MINIMUM ENERGY HYPERSONIC NOSE AND LEADING EDGE SHAPES, by Roger J. Furey. Wash., Sep 1969. vi, 43p. illus., refs. (Aerodynamics Laboratory. Aero Rpt. 1164. Aero Problem 648-240) (NASC Project WR 009 0201) UNCLASSIFIED

A system of first-order differential equations governing the heat transfer (convection and shock layer radiation) and pressure drag of an axisymmetric or two-dimensional body in hypersonic flow is developed. The Pontryagin Maximum Principle is applied to this system, through the gradient method, and a series of optimum hypersonic nose and two-dimensional shapes of given fineness ratio is found. The axisymmetric minimum drag shape is similar to the familiar 3/4 power law profile while the two-dimensional result is wedge shaped. The minimum

Drag, Minimum
Drag, Hypersonic
Heat Transfer, Minimum
Heat Transfer, Hypersonic
Heat Transfer--Bodies, Blunt
Heat Transfer--Bodies, Two-Dimensional
Heat Transfer--Bodies, Axisymmetric
Wings--Thickness, Leading Edge
Airplanes, Hypersonic--Design

Naval Ship R&D Center. Report 3186.
MINIMUM ENERGY HYPERSONIC NOSE AND LEADING EDGE SHAPES, by Roger J. Furey. Wash., Sep 1969. vi, 43p. illus., refs. (Aerodynamics Laboratory. Aero Rpt. 1164. Aero Problem 648-240) (NASC Project WR 009 0201) UNCLASSIFIED

A system of first-order differential equations governing the heat transfer (convection and shock layer radiation) and pressure drag of an axisymmetric or two-dimensional body in hypersonic flow is developed. The Pontryagin Maximum Principle is applied to this system, through the gradient method, and a series of optimum hypersonic nose and two-dimensional shapes of given fineness ratio is found. The axisymmetric minimum drag shape is similar to the familiar 3/4 power law profile while the two-dimensional result is wedge shaped. The minimum

Drag, Minimum
Drag, Hypersonic
Heat Transfer, Minimum
Heat Transfer, Hypersonic
Heat Transfer--Bodies, Blunt
Heat Transfer--Bodies, Two-Dimensional
Heat Transfer--Bodies, Axisymmetric
Wings--Thickness, Leading Edge
Airplanes, Hypersonic--Design

heat transfer profiles are found to be flat faced when considering convection alone and conical, with a cusped tip, when considering radiation alone. Minimum energy shapes are found wherein the various energy terms being minimized include the sum of convection plus drag work, convection plus radiation plus drag work and convection plus radiation. The axisymmetric results show reasonable accommodation for the various energy forms considered in each of the minimum energy nose shapes. The two-dimensional minimum energy shapes are found to be dominated by the drag work with the results being, for all practical purposes, wedge shaped.

Numerical Calculations
(Maximum Principle)

Furey, Roger J.
Catholic U Thesis
NSRDC Aero Rpt 1164
NSRDC Aero Test C-240
NASC Proj WR 009 0201

heat transfer profiles are found to be flat faced when considering convection alone and conical, with a cusped tip, when considering radiation alone. Minimum energy shapes are found wherein the various energy terms being minimized include the sum of convection plus drag work, convection plus radiation plus drag work and convection plus radiation. The axisymmetric results show reasonable accommodation for the various energy forms considered in each of the minimum energy nose shapes. The two-dimensional minimum energy shapes are found to be dominated by the drag work with the results being, for all practical purposes, wedge shaped.

Numerical Calculations
(Maximum Principle)

Furey, Roger J.
Catholic U Thesis
NSRDC Aero Rpt 1164
NSRDC Aero Test C-240
NASC Proj WR 009 0201

heat transfer profiles are found to be flat faced when considering convection alone and conical, with a cusped tip, when considering radiation alone. Minimum energy shapes are found wherein the various energy terms being minimized include the sum of convection plus drag work, convection plus radiation plus drag work and convection plus radiation. The axisymmetric results show reasonable accommodation for the various energy forms considered in each of the minimum energy nose shapes. The two-dimensional minimum energy shapes are found to be dominated by the drag work with the results being, for all practical purposes, wedge shaped.

Numerical Calculations
(Maximum Principle)

Furey, Roger J.
Catholic U Thesis
NSRDC Aero Rpt 1164
NSRDC Aero Test C-240
NASC Proj WR 009 0201

heat transfer profiles are found to be flat faced when considering convection alone and conical, with a cusped tip, when considering radiation alone. Minimum energy shapes are found wherein the various energy terms being minimized include the sum of convection plus drag work, convection plus radiation plus drag work and convection plus radiation. The axisymmetric results show reasonable accommodation for the various energy forms considered in each of the minimum energy nose shapes. The two-dimensional minimum energy shapes are found to be dominated by the drag work with the results being, for all practical purposes, wedge shaped.

Numerical Calculations
(Maximum Principle)

Furey, Roger J.
Catholic U Thesis
NSRDC Aero Rpt 1164
NSRDC Aero Test C-240
NASC Proj WR 009 0201

Naval Ship R&D Center. Report 3186.
MINIMUM ENERGY HYPERSONIC NOSE AND LEADING EDGE SHAPES, by Roger J. Furey. Wash., Sep 1969. vi, 43p. illus., refs. (Aerodynamics Laboratory. Aero Rpt. 1164. Aero Problem 648-240) (NASC Project WR 009 0201) UNCLASSIFIED

A system of first-order differential equations governing the heat transfer (convection and shock layer radiation) and pressure drag of an axisymmetric or two-dimensional body in hypersonic flow is developed. The Pontryagin Maximum Principle is applied to this system, through the gradient method, and a series of optimum hypersonic nose and two-dimensional shapes of given fineness ratio is found. The axisymmetric minimum drag shape is similar to the familiar 3/4 power law profile while the two-dimensional result is wedge shaped. The minimum

Drag, Minimum
Drag, Hypersonic
Heat Transfer, Minimum
Heat Transfer, Hypersonic
Heat Transfer--Bodies, Blunt
Heat Transfer--Bodies, Two-Dimensional
Heat Transfer--Bodies, Axisymmetric
Wings--Thickness, Leading Edge
Airplanes, Hypersonic--Design

Naval Ship R&D Center. Report 3186.
MINIMUM ENERGY HYPERSONIC NOSE AND LEADING EDGE SHAPES, by Roger J. Furey. Wash., Sep 1969. vi, 43p. illus., refs. (Aerodynamics Laboratory. Aero Rpt. 1164. Aero Problem 648-240) (NASC Project WR 009 0201) UNCLASSIFIED

A system of first-order differential equations governing the heat transfer (convection and shock layer radiation) and pressure drag of an axisymmetric or two-dimensional body in hypersonic flow is developed. The Pontryagin Maximum Principle is applied to this system, through the gradient method, and a series of optimum hypersonic nose and two-dimensional shapes of given fineness ratio is found. The axisymmetric minimum drag shape is similar to the familiar 3/4 power law profile while the two-dimensional result is wedge shaped. The minimum

Drag, Minimum
Drag, Hypersonic
Heat Transfer, Minimum
Heat Transfer, Hypersonic
Heat Transfer--Bodies, Blunt
Heat Transfer--Bodies, Two-Dimensional
Heat Transfer--Bodies, Axisymmetric
Wings--Thickness, Leading Edge
Airplanes, Hypersonic--Design

Naval Ship R&D Center. Report 3186.
MINIMUM ENERGY HYPERSONIC NOSE AND LEADING EDGE SHAPES, by Roger J. Furey. Wash., Sep 1969. vi, 43p. illus., refs. (Aerodynamics Laboratory. Aero Rpt. 1164. Aero Problem 648-240) (NASC Project WR 009 0201) UNCLASSIFIED

A system of first-order differential equations governing the heat transfer (convection and shock layer radiation) and pressure drag of an axisymmetric or two-dimensional body in hypersonic flow is developed. The Pontryagin Maximum Principle is applied to this system, through the gradient method, and a series of optimum hypersonic nose and two-dimensional shapes of given fineness ratio is found. The axisymmetric minimum drag shape is similar to the familiar 3/4 power law profile while the two-dimensional result is wedge shaped. The minimum

Drag, Minimum
Drag, Hypersonic
Heat Transfer, Minimum
Heat Transfer, Hypersonic
Heat Transfer--Bodies, Blunt
Heat Transfer--Bodies, Two-Dimensional
Heat Transfer--Bodies, Axisymmetric
Wings--Thickness, Leading Edge
Airplanes, Hypersonic--Design

Naval Ship R&D Center. Report 3186.
MINIMUM ENERGY HYPERSONIC NOSE AND LEADING EDGE SHAPES, by Roger J. Furey. Wash., Sep 1969. vi, 43p. illus., refs. (Aerodynamics Laboratory. Aero Rpt. 1164. Aero Problem 648-240) (NASC Project WR 009 0201) UNCLASSIFIED

A system of first-order differential equations governing the heat transfer (convection and shock layer radiation) and pressure drag of an axisymmetric or two-dimensional body in hypersonic flow is developed. The Pontryagin Maximum Principle is applied to this system, through the gradient method, and a series of optimum hypersonic nose and two-dimensional shapes of given fineness ratio is found. The axisymmetric minimum drag shape is similar to the familiar 3/4 power law profile while the two-dimensional result is wedge shaped. The minimum

Drag, Minimum
Drag, Hypersonic
Heat Transfer, Minimum
Heat Transfer, Hypersonic
Heat Transfer--Bodies, Blunt
Heat Transfer--Bodies, Two-Dimensional
Heat Transfer--Bodies, Axisymmetric
Wings--Thickness, Leading Edge
Airplanes, Hypersonic--Design

heat transfer profiles are found to be flat faced when considering convection alone and conical, with a cusped tip, when considering radiation alone. Minimum energy shapes are found wherein the various energy terms being minimized include the sum of convection plus drag work, convection plus radiation plus drag work and convection plus radiation. The axisymmetric results show reasonable accommodation for the various energy forms considered in each of the minimum energy nose shapes. The two-dimensional minimum energy shapes are found to be dominated by the drag work with the results being, for all practical purposes, wedge shaped.

Numerical Calculations
(Maximum Principle)

Furey, Roger J.
Catholic U Thesis
NSRDC Aero Rpt 1164
NSRDC Aero Test C-240
NASC Proj WR 009 0201

heat transfer profiles are found to be flat faced when considering convection alone and conical, with a cusped tip, when considering radiation alone. Minimum energy shapes are found wherein the various energy terms being minimized include the sum of convection plus drag work, convection plus radiation plus drag work and convection plus radiation. The axisymmetric results show reasonable accommodation for the various energy forms considered in each of the minimum energy nose shapes. The two-dimensional minimum energy shapes are found to be dominated by the drag work with the results being, for all practical purposes, wedge shaped.

Numerical Calculations
(Maximum Principle)

Furey, Roger J.
Catholic U Thesis
NSRDC Aero Rpt 1164
NSRDC Aero Test C-240
NASC Proj WR 009 0201

heat transfer profiles are found to be flat faced when considering convection alone and conical, with a cusped tip, when considering radiation alone. Minimum energy shapes are found wherein the various energy terms being minimized include the sum of convection plus drag work, convection plus radiation plus drag work and convection plus radiation. The axisymmetric results show reasonable accommodation for the various energy forms considered in each of the minimum energy nose shapes. The two-dimensional minimum energy shapes are found to be dominated by the drag work with the results being, for all practical purposes, wedge shaped.

Numerical Calculations
(Maximum Principle)

Furey, Roger J.
Catholic U Thesis
NSRDC Aero Rpt 1164
NSRDC Aero Test C-240
NASC Proj WR 009 0201

heat transfer profiles are found to be flat faced when considering convection alone and conical, with a cusped tip, when considering radiation alone. Minimum energy shapes are found wherein the various energy terms being minimized include the sum of convection plus drag work, convection plus radiation plus drag work and convection plus radiation. The axisymmetric results show reasonable accommodation for the various energy forms considered in each of the minimum energy nose shapes. The two-dimensional minimum energy shapes are found to be dominated by the drag work with the results being, for all practical purposes, wedge shaped.

Numerical Calculations
(Maximum Principle)

Furey, Roger J.
Catholic U Thesis
NSRDC Aero Rpt 1164
NSRDC Aero Test C-240
NASC Proj WR 009 0201